Adv Comput Math (2022) 48: 49
https://doi.org/10.1007/s10444-022-09938-2

Adaptive finite element approximation for steady-state Poisson-Nernst-Planck equations

Tingting Hao[1,2] · Manman Ma[1] · Xuejun Xu[1,3]

Received: 15 February 2021 / Accepted: 24 February 2022 / Published online: 22 July 2022

Abstract

In this paper, we develop an adaptive finite element method for the nonlinear steady-state Poisson-Nernst-Planck equations, where the spatial adaptivity for geometrical singularities and boundary layer effects are mainly considered. As a key contribution, the steady-state Poisson-Nernst-Planck equations are studied systematically and rigorous analysis for a residual-based a posteriori error estimate of the nonlinear system is presented. With the regularity of the linearized system derived by taking G-derivatives of the nonlinear system, we show the robust relationship between the error of solution and the a posteriori error estimator. Numerical experiments are given to validate the efficiency of the a posteriori error estimator and demonstrate the expected rate of convergence. In further tests, adaptive mesh refinements for geometrical singularities and boundary layer effects are successfully observed.

Keywords Poisson-nernst-planck equations · A posteriori error estimate · Adaptive finite element method · Boundary layer effects

Mathematics Subject Classification (2010) 65N15 · 65N30 · 65J15 · 35K61

Communicated by: Paul Houston

✉ Manman Ma
mamm@tongji.edu.cn

Tingting Hao
1710386@tongji.edu.cn

Xuejun Xu
xxj@lsec.cc.ac.cn

[1] School of Mathematical Sciences, Tongji University, Shanghai 200092, China

[2] HUA LOOKENG Honors College, Changzhou University, Changzhou 213164, China

[3] LSEC, Institute of Computational Mathematics and Scientific/Engineering Computing, Academy of Mathematics and System Sciences, Chinese Academy of Sciences, Beijing 100190, China

1 Introduction

In this work, we consider the steady-state Poisson-Nernst-Planck (PNP) equations

$$\begin{cases} -\nabla \cdot D_i(\nabla c_i + \beta z_i e c_i \nabla \psi) = F_i, \ i = 1, ..., K, \\ -\nabla \cdot (\varepsilon_r \varepsilon_0 \nabla \psi) - \sum_{i=1}^{K} z_i e c_i = F^f, \end{cases} \tag{1}$$

which describe the nonlinear coupling of the electric potential ψ and the ionic concentration c_i of the ith species. The first equation is called the Nernst-Planck equation for species i and the second one is the named the Poisson's equation. Here, D_i and z_i are the diffusivity and valence, respectively. $\beta = 1/(k_B T_{abs})$, with k_B the Boltzmann constant and T_{abs} the absolute temperature. e is the elementary charge, ε_r and ε_0 are the relative and vacuum dielectric permittivities, F_i denotes the reaction source term, and F^f is generally due to the fixed charges. The Debye length is then defined as $\ell_D = [\varepsilon_r \varepsilon_0/(\beta \sum_{i=1}^{K} z_i^2 e^2 c_i^b)]^{1/2}$ with c_i^b the ith bulk concentration. Furthermore, the boundary layer effects can be described by the dimensionless parameter $\epsilon = 2(\ell_D/l_0)^2$ with l_0 the characteristic length of the considered domain.

Despite the fact that the PNP system has been well known and widely studied for over a century because of its physical applications such as semiconductor studies [11, 24, 47] and electrodiffusion problems [20, 34, 45], it is attracting more attentions as being used to describe the dynamics of ion transport in biological membrane channels [43, 55, 60, 65]. Recently, modified models beyond mean field theory such as incorporating ionic steric effects, correlation effects and inhomogeneous dielectric effects have been extensively studied with great interests [32, 37, 38, 44, 66]. For early theoretical analysis, Jerome [35] and Hayeck et al. [28] proved the existence of solutions for steady-state PNP according to Schauder fixed point theorem, while Mock [49], Brezzi et al. [10], and Gajewski [23] gave out the conclusion of uniqueness under some local constraints. Due to the strong coupling and high nonlinearity, the analytical or asymptotic solutions of PNP equations have been only studied for simple 1-D [27] or single-ion-species cases [51]. More analytical results for steady-state PNP equations are referred to [5, 26, 42, 52] where only 1-D cases are considered. As a result, the steady or unsteady PNP equations are in general solved numerically with regular computational domains.

A variety of numerical methods have been used extensively for solving PNP equations, which can be broadly categorized as using finite difference method [7, 13, 19, 33, 41, 71], finite element method [25, 29, 36, 43, 53, 54, 72], finite volume method [46, 61], the boundary element method [72], and the spectrum method [30]. Among those numerical approaches, finite element methods have been known to perform well for more irregular geometries and complicated boundaries. With the increasing computing capabilities and numerical improvements, the PNP model has been applied recently in simulating large systems such as practical biophysical system; nevertheless, the computational costs of classical methods with uniform meshes are still expensive. Additionally, the boundary layer effect due to thin Debye layer, the singularity of Dirac charge distribution sources, and geometrical singularities cause

significant difficulties in obtaining required numerical accuracy when standard methods are used. Although singular perturbation treatments have been applied to the PNP system for thin Debye layer limit [42], very few efficient numerical analysis aiming at overcoming those singularities has been proposed to the best of our knowledge. As a special equilibrium state of PNP equation, the nonlinear Poisson-Boltzmann (PB) equation with Dirac charge distribution has been systematically discussed and adaptive finite element approximations have been developed in previous works [16, 31]. Later on, a parallel adaptive finite element algorithm of the steady-state PNP has been developed with using an a posteriori error estimator which is similar to that in PB [62]. However, PB has reduced the strongly coupled system into a single equation and simplified the nonlinear difficulties of PNP system itself. Besides, the above-mentioned singularities and boundary layer effects require more general adaptive numerical analysis for PNP equations.

The analysis of adaptive finite element methods has made important progress in understanding the basic principles in recent years. Typical adaptive algorithms provide an automatic feedback routine with successive loops of the structure: $SOLVE \rightarrow ESTIMATE \rightarrow MARK \rightarrow REFINE$, of which "*ESTIMATE*" is to find out where correction is needed through the a posteriori error estimator η, so as to prepare for grid-marking and mesh refinement. The adaptive finite element method is able to drive local refinement by a posteriori error estimation and achieve the mesh adaptation, which can well resolve the geometrical singularities, boundary layer effects, and so on. Meanwhile, the a posteriori error estimates determine the error control that depends on the numerical solutions only. A posteriori error estimation varies for different equations [14, 22, 56] and multiple a posteriori error estimates can exist even for the same problem [3].

In this work, a posteriori error estimates are mainly considered for analyzing the PNP equations, however, the nonlinearity and strong coupling of the system lead to great difficulties in obtaining the estimates as following the classical a posteriori error estimation of the residual type [58] where the a posteriori error estimates can be achieved by considering the original equation system directly. Fortunately, a general solution for the a posteriori error estimates of nonlinear elliptic equations was developed by Verfürth [57] decades ago and was further discussed by Ainsworth and Oden in Ref. [3]. Solving PNP equations becomes a singular perturbation problem with the small dimensionless parameter ϵ that describes the boundary layer effects. Although there are many studies on the a posterior estimation of linear singular perturbation problems with considering the boundary layer effects [2, 4, 15, 18, 69, 70], to solve corresponding cases with nonlinear and strongly coupling problems is challenging as satisfying the robustness of the estimation. Here, the robustness means the estimators yield upper and lower bounds on the error such that the ratio of the upper and lower bounds is bounded from below and from above by constants which are independent of any mesh size and the small perturbation parameter ϵ [59]. The current work proposes the a posteriori error estimate of PNP equations and proves both its reliability and efficiency. Furthermore, the robustness of the estimator is demonstrated with defining an improved ϵ-dependent norm of error inspired by the coupling between unknowns in PNP equations.

The paper is organized as follows. We begin in Section 2 by defining the PNP system, its variational form, and the finite element spaces to be used. In Section 3, we develop the a posteriori error estimate with demonstrating its reliability and efficiency. In Section 4, numerical experiments are reported to show the accuracy of the adaptive method and agreements to theorems of the a posteriori error estimation. Conclusion remarks are finally made in Section 5.

2 Preliminary

Let $\Omega \subset R^2$ be a bounded convex Lipschitz domain. We use standard notations for Sobolev spaces $W^{1,2}(\Omega) = H^1(\Omega)$, and the associated norms and seminorms. Here, $H_0^1(\Omega) = \{v \in H^1(\Omega) : v|_{\partial\Omega} = 0\}$ and $H^{-1}(\Omega) = (H_0^1(\Omega))^*$ which means the dual space of $H_0^1(\Omega)$. In all proofs, $a \lesssim b$ means $a \leq Cb$ where C is a constant.

2.1 PNP system and its variational form

For simplicity, the 1:1 symmetric system is considered in this work, i.e., $K = 2$, $z_1 = -z_2 = 1$ and $D_1 = D_2$, with $c_1 = p$ and $c_2 = n$ denoting the positive and negative ionic concentration, respectively. The general steady-state PNP is then reduced to the dimensionless form as follows:

$$\begin{cases} -\Delta p - \nabla \cdot (p\nabla\psi) = f_1, \\ -\Delta n + \nabla \cdot (n\nabla\psi) = f_2, \\ -\epsilon\Delta\psi = p - n + f_3, \end{cases} \tag{2}$$

with ϵ being defined below Eq. (1). In this work, we take $\epsilon \in (0, 1]$ where small ϵ values correspond to cases with boundary layer effects, or namely thin Debye layer effects. Alternatively, the system (2) can be written as a general system $\boldsymbol{F}(\boldsymbol{u}) = \boldsymbol{0}$ with $\boldsymbol{u}(\boldsymbol{x}) = (p(\boldsymbol{x}), n(\boldsymbol{x}), \psi(\boldsymbol{x}))$, and is satisfied by $p(\boldsymbol{x}), n(\boldsymbol{x})$ and $\psi(\boldsymbol{x}) \in H^1(\Omega)$ on the two dimensional domain considered in current work, i.e., $\boldsymbol{x} = (x, y) \in \Omega$. Let $\boldsymbol{f}(\boldsymbol{x}) = (f_1, f_2, f_3) \in (L^2(\Omega))^3$. For simplicity, we consider the following homogeneous Dirichlet boundary conditions,

$$p = n = \psi = 0, \text{ on } \partial\Omega. \tag{3}$$

Hence, the weak formulation of system (2) is,

$$\int_\Omega (v_1, v_2, v_3) \begin{pmatrix} -\Delta p - \nabla \cdot (p\nabla\psi) \\ -\Delta n + \nabla \cdot (n\nabla\psi) \\ -\epsilon\Delta\psi - p + n \end{pmatrix} d\boldsymbol{x} = \int_\Omega (v_1, v_2, v_3) \begin{pmatrix} f_1 \\ f_2 \\ f_3 \end{pmatrix} d\boldsymbol{x}, \tag{4}$$

then, $\boldsymbol{u} = (p, n, \psi) \in (H_0^1(\Omega))^3$ is the weak solution of (2) if and only if $\forall \boldsymbol{v} = (v_1, v_2, v_3) \in (H_0^1(\Omega))^3$, $\boldsymbol{u}$ satisfies,

$$\begin{aligned} < \boldsymbol{F}(\boldsymbol{u}), \boldsymbol{v} > &= \int_\Omega (\nabla p \cdot \nabla v_1 + p\nabla\psi \cdot \nabla v_1 + \nabla n \cdot \nabla v_2 - n\nabla\psi \cdot \nabla v_2 + \epsilon\nabla\psi \cdot \nabla v_3 \\ &\quad - pv_3 + nv_3 - f_1 v_1 - f_2 v_2 - f_3 v_3) d\boldsymbol{x} \\ &= 0. \end{aligned} \tag{5}$$

Note that $\boldsymbol{F}$ is a nonlinear operator here from $(H_0^1(\Omega))^3$ to $(H^{-1}(\Omega))^3$.

Next, we propose the linear problem by introducing the G-derivative ($G\hat{a}teaux$ derivative [68]) operator $DF(\cdot)$ at $\boldsymbol{u}$ as follows,

$$< DF(\boldsymbol{u})\boldsymbol{\phi}, \boldsymbol{w} >= \lim_{\hat{\varepsilon}\to 0} \frac{< \boldsymbol{F}(\boldsymbol{u}+\hat{\varepsilon}\boldsymbol{\phi}) - \boldsymbol{F}(\boldsymbol{u}), \boldsymbol{w} >}{\hat{\varepsilon}}, \ \forall \boldsymbol{\phi}, \boldsymbol{w} \in (H_0^1(\Omega))^3, \quad (6)$$

which leads to the following linear problem:

To find $\boldsymbol{\phi} = (\phi_1, \phi_2, \phi_3) \in (H_0^1(\Omega))^3$, $\forall \boldsymbol{R} \in (L^2(\Omega))^3$, such that,

$$< DF(\boldsymbol{u})\boldsymbol{\phi}, \boldsymbol{v} >=< \boldsymbol{R}, \boldsymbol{v} >, \quad \forall \boldsymbol{v} \in (H_0^1(\Omega))^3, \quad (7)$$

where $\boldsymbol{u}$ satisfies (5). The well-posedness of the linear problem (7) has been verified in [8].

2.2 Finite element discretization

Let the regular partition of Ω be $\mathcal{T}_h$ with the mesh size $0 < h < 1$ [9] and the corresponding finite element space be $V_h = \{v \in H_0^1(\Omega) : v|_\tau \in \mathcal{P}_1(\tau), \forall \tau \in \mathcal{T}_h\}$. We define $\boldsymbol{u}_h := (p_h, n_h, \psi_h) \in (V_h)^3$.

The finite element approximation of (5) is to find $\boldsymbol{u}_h \in (V_h)^3$ satisfying,

$$< \boldsymbol{F}(\boldsymbol{u}_h), \boldsymbol{v}_h >= 0, \ \forall \boldsymbol{v}_h = (v_{h,1}, v_{h,2}, v_{h,3}) \in (V_h)^3, \quad (8)$$

which based on (5) gives

$$\begin{aligned} & < \boldsymbol{F}(\boldsymbol{u}_h), \boldsymbol{v}_h > \\ = & \int_\Omega (\nabla p_h \cdot \nabla v_{h,1} + p_h \nabla \psi_h \cdot \nabla v_{h,1} + \nabla n_h \cdot \nabla v_{h,2} - n_h \nabla \psi_h \cdot \nabla v_{h,2} \\ & + \epsilon \nabla \psi_h \cdot \nabla v_{h,3} - p_h v_{h,3} + n_h v_{h,3} - f_1 v_{h,1} - f_2 v_{h,2} - f_3 v_{h,3}) dx. \end{aligned} \quad (9)$$

3 The construction of an a posteriori error estimator

The ϵ-dependent norm, $||\cdot||_{\epsilon,\Omega}$, is defined as referring to the energy norm, i.e., $\forall \phi \in H^1(\Omega)$,

$$||\phi||_{\epsilon,\Omega} = \left(\|\phi\|_{L^2(\Omega)}^2 + \epsilon |\phi|_{1,\Omega}^2 \right)^{1/2},$$

and

$$||u||_{\epsilon,\Omega} = \left(\|p\|_{1,\Omega}^2 + \|n\|_{1,\Omega}^2 + \|\psi\|_\epsilon^2 \right)^{1/2}.$$

See similar treatment in [59]. We further define

$$\|f\|_{-\epsilon,\Omega} = \sup_{0\neq v\in H_0^1(\Omega)} \frac{|< f, v >|}{\|v\|_{\epsilon,\Omega}}, \quad \|\boldsymbol{F}\|_{-\epsilon,\Omega} = \sup_{\boldsymbol{0}\neq \boldsymbol{v}\in (H_0^1(\Omega))^3} \frac{|< \boldsymbol{F}, \boldsymbol{v} >|}{\|\boldsymbol{v}\|_{\epsilon,\Omega}}, \quad (10)$$

$\forall f \in H^{-1}(\Omega)$ and $\forall \boldsymbol{F} \in ((H_0^1(\Omega))^3)^*$.

In order to obtain robust a posteriori estimate, we go one step further to define an improved energy norm as follows,

$$||u||_{*,\Omega} = ||u||_{\epsilon,\Omega} + ||u||_{1,\Omega}.$$

The key part of the process "*ESTIMATE*" in adaptive finite element algorithm is to find an a posteriori error estimator η and establish the relationship between η and the absolute error of solution, $\boldsymbol{e} = \boldsymbol{u} - \boldsymbol{u}_h := (e_1, e_2, e_3) \in (H_0^1(\Omega))^3$, as following:

$$\underline{C}\eta \leq \|\boldsymbol{e}\|_* \leq \overline{C}\eta, \tag{11}$$

with the constants $\underline{C}$ and $\overline{C}$ independent of $\boldsymbol{u}_h$ and $\boldsymbol{f}$. Here, the lower and upper bounds are called the efficiency and reliability of the a posteriori error estimator, respectively.

In order to prove inequality (11), we split the process into two steps, which are the a posteriori error analysis for upper and lower bounds on the error, respectively. Furthermore, we show $\overline{C}$ and $\underline{C}$ do not depend on ϵ, that is, the error estimation is robust.

3.1 Upper bounds of the error

Before illustrating the upper bounding relationship, we show the regularity of the linear problem (7).

Lemma 1 *If $p, n \in L^\infty(\Omega)$, we have the regularity conclusion for* Eq. (7) *as follows,*

$$\|\boldsymbol{\phi}\|_{\epsilon,\Omega} \leq M_1 \|\boldsymbol{R}\|_{-\epsilon,\Omega}, \quad \forall \boldsymbol{R} \in (L^2(\Omega))^3, \tag{12}$$

where the constant M_1 depends on the exact solution of system (2) *but is independent of $\boldsymbol{\phi}$, $\boldsymbol{R}$ and ϵ.*

Proof Eqs. (5) and (6) lead to the variational form of Eq. (7) as

$$\begin{aligned} & < \boldsymbol{DF}(\boldsymbol{u})\boldsymbol{\phi}, \boldsymbol{v} > \\ = & \int_\Omega (\nabla\phi_1 \cdot \nabla v_1 + p\nabla\phi_3 \cdot \nabla v_1 + \phi_1 \nabla\psi \cdot \nabla v_1 + \nabla\phi_2 \cdot \nabla v_2 \\ & -n\nabla\phi_3 \cdot \nabla v_2 - \phi_2 \nabla\psi \cdot \nabla v_2 + \epsilon\nabla\phi_3 \cdot \nabla v_3 - \phi_1 v_3 + \phi_2 v_3) dx. \end{aligned} \tag{13}$$

Based on the regularity of ψ and embedded theorem [1, 40], we have $\psi \in W^{1,\infty}(\Omega)$ for $\Omega \subset R^2$, that is, $\|\psi\|_{W^{1,\infty}(\Omega)} \lesssim \|\psi\|_{H^2(\Omega)} \lesssim \|p - n + f_3\|_{L^2(\Omega)} < \infty$. Owing to $Cauchy - Schwarz$ and $H\ddot{o}lder$ inequality, we have

$$\begin{aligned} & | < \boldsymbol{DF}(\boldsymbol{u})\boldsymbol{\phi}, \boldsymbol{v} > | \\ \lesssim & |\phi_1|_{1,\Omega}|v_1|_{1,\Omega} + |\phi_3|_{1,\Omega}|v_1|_{1,\Omega} + \|\phi_1\|_{L^2(\Omega)}|v_1|_{1,\Omega} \\ & + |\phi_2|_{1,\Omega}|v_2|_{1,\Omega} + |\phi_3|_{1,\Omega}|v_2|_{1,\Omega} + \|\phi_2\|_{L^2(\Omega)}|v_2|_{L^2(\Omega)} \\ & + \epsilon|\phi_3|_{1,\Omega}|v_3|_{1,\Omega} + \|\phi_1\|_{L^2(\Omega)}\|v_3\|_{L^2(\Omega)} + \|\phi_2\|_{L^2(\Omega)}\|v_3\|_{L^2(\Omega)} \\ \lesssim & \|\boldsymbol{\phi}\|_{1,\Omega}\|\boldsymbol{v}\|_{1,\Omega}, \end{aligned} \tag{14}$$

where the ϵ-dependence has been eliminated due to the assumption $p, n \in L^\infty(\Omega)$.

Besides, we have the one-to-one mapping $\boldsymbol{DF}(\boldsymbol{u}) : (H_0^1(\Omega))^3 \to (L^2(\Omega))^3$ due to the conclusions in [8]. By the bounded inverse theorem there exists an inverse

$\boldsymbol{DF}(\boldsymbol{u})^{-1} : (L^2(\Omega))^3 \to (H_0^1(\Omega))^3$, and by the Hahn-Banach theorem there exists a linear extension $\boldsymbol{G} : (H^{-1}(\Omega))^3 \to (H_0^1(\Omega))^3$ satisfying $\boldsymbol{G}|_{(L^2(\Omega))^3} = \boldsymbol{DF}(\boldsymbol{u})^{-1}$ and $\|\boldsymbol{G}\| = \|\boldsymbol{DF}(\boldsymbol{u})^{-1}\|$. Moreover, $\|\boldsymbol{DF}(\boldsymbol{u})^{-1}\| \le M_1$ where the constant M_1 depends on the exact solution of system (2) only and is independent of ϵ. Thus, $\forall \boldsymbol{R} \in (L^2(\Omega))^3 \subset (H^{-1}(\Omega))^3$,

$$\|\boldsymbol{\phi}\|_{1,\Omega} = \|\boldsymbol{GR}\|_{1,\Omega} \le \|\boldsymbol{DF}(\boldsymbol{u})^{-1}\|\|\boldsymbol{R}\|_{-1,\Omega} \le M_1\|\boldsymbol{R}\|_{-1,\Omega}. \tag{15}$$

Then, with $\|\boldsymbol{\phi}\|_{\epsilon,\Omega} \le \|\boldsymbol{\phi}|_{1,\Omega}$ and $\|\boldsymbol{R}\|_{-1,\Omega} \le \|\boldsymbol{R}\|_{-\epsilon,\Omega}$, we have the inequality (12). □

Theorem 1 *If $p, n \in L^\infty(\Omega)$, and the error $\boldsymbol{e}$ is small enough, that is $\|\nabla e_3\|_{L^\infty(\Omega)} \le 1/(2\sqrt{2}M_1)$, then,*

$$\|\boldsymbol{e}\|_{\epsilon,\Omega} \le 2M_1\|\boldsymbol{F}(\boldsymbol{u}_h)\|_{-\epsilon,\Omega}. \tag{16}$$

Here, M_1 is the same constant in Lemma 1.

Proof The definition of G-derivative [68] indicates that, $\forall \boldsymbol{w} \in (H_0^1(\Omega))^3$,

$$\int_0^1 < \boldsymbol{DF}(\boldsymbol{u} + t\boldsymbol{e})\boldsymbol{e}, \boldsymbol{w} > dt = < \boldsymbol{F}(\boldsymbol{u}_h), \boldsymbol{w} > - < \boldsymbol{F}(\boldsymbol{u}), \boldsymbol{w} > . \tag{17}$$

By means of the fact that $< \boldsymbol{F}(\boldsymbol{u}), \boldsymbol{w} >= 0,\ \forall \boldsymbol{w} \in (H_0^1(\Omega))^3$, we have

$$< \boldsymbol{F}(\boldsymbol{u}_h), \boldsymbol{w} >= \int_0^1 < \boldsymbol{DF}(\boldsymbol{u} + t\boldsymbol{e})\boldsymbol{e}, \boldsymbol{w} > dt, \tag{18}$$

and thus,

$$< \boldsymbol{DF}(\boldsymbol{u})\boldsymbol{e}, \boldsymbol{w} >= \int_0^1 <\boldsymbol{DF}(\boldsymbol{u})\boldsymbol{e} - \boldsymbol{DF}(\boldsymbol{u} + t\boldsymbol{e})\boldsymbol{e}, \boldsymbol{w} > dt + < \boldsymbol{F}(\boldsymbol{u}_h), \boldsymbol{w} > . \tag{19}$$

We now define $< \boldsymbol{DF}(\boldsymbol{u})\boldsymbol{e}, \boldsymbol{w} >=< \widetilde{\boldsymbol{R}}, \boldsymbol{w} >$ for convenience. The inequality (12) now leads to $\|\boldsymbol{e}\|_{\epsilon,\Omega} \le M_1||\widetilde{\boldsymbol{R}}||_{-\epsilon,\Omega}$ as taking $\boldsymbol{\phi} = \boldsymbol{e}$.

Next, the integral part in (19) is estimated, i.e.,

$$\begin{aligned}
&| < \boldsymbol{DF}(\boldsymbol{u})\boldsymbol{e} - \boldsymbol{DF}(\boldsymbol{u} + t\boldsymbol{e})\boldsymbol{e}, \boldsymbol{w} > | \\
&= 2t\left|\int_\Omega (e_1\nabla e_3 \cdot \nabla w_1 - e_2\nabla e_3 \cdot \nabla w_2)dx\right| \\
&\le 2\sqrt{2}t\|\nabla e_3\|_{L^\infty(\Omega)}(||e_1||_{L^2(\Omega)}||\nabla w_1||_{L^2(\Omega)} + ||e_1||_{L^2(\Omega)}||\nabla w_2||_{L^2(\Omega)}) \\
&\le 2\sqrt{2}t\|\nabla e_3\|_{L^\infty(\Omega)}\|\boldsymbol{e}\|_{\epsilon,\Omega}\|\boldsymbol{w}\|_{\epsilon,\Omega},
\end{aligned} \tag{20}$$

where the $Cauchy-Schwarz$ and $H\ddot{o}lder$ inequality are used, and hence

$$\begin{aligned}
&\|\boldsymbol{e}\|_{\epsilon,\Omega}\\
\leq\ & M_1||\widetilde{\boldsymbol{R}}||_{-\epsilon,\Omega}\\
\leq\ & M_1 \sup_{\|\boldsymbol{w}\|_{\epsilon,\Omega}=1}\left(\left|\int_0^1 <\boldsymbol{DF}(\boldsymbol{u})\boldsymbol{e}-\boldsymbol{DF}(\boldsymbol{u}+t\boldsymbol{e})\boldsymbol{e},\boldsymbol{w}>dt\right|+|<\boldsymbol{F}(\boldsymbol{u}_h),\boldsymbol{w}>|\right)\\
\leq\ & M_1 \sup_{\|\boldsymbol{w}\|_{\epsilon,\Omega}=1}(\sqrt{2}\|\nabla e_3\|_{L^\infty(\Omega)}\|\boldsymbol{e}\|_{\epsilon,\Omega}\|\boldsymbol{w}\|_{\epsilon,\Omega})+M_1\|F(\boldsymbol{u}_h)\|_{-\epsilon,\Omega}\\
=\ & \sqrt{2}M_1\|\nabla e_3\|_{L^\infty(\Omega)}\|\boldsymbol{e}\|_{\epsilon,\Omega}+M_1\|F(\boldsymbol{u}_h)\|_{-\epsilon,\Omega}. \qquad (21)
\end{aligned}$$

Notably, we shall have $\|\boldsymbol{e}\|_{\epsilon,\Omega}\lesssim\|\boldsymbol{F}(\boldsymbol{u}_h)\|_{-\epsilon,\Omega}$ if $\|\nabla e_3\|_{L^\infty(\Omega)}<1/\left(\sqrt{2}M_1\right)$, however, we restrict the condition as $\|\nabla e_3\|_{L^\infty(\Omega)}\leq 1/(2\sqrt{2}M_1)$ for convenience, and obtain

$$\|\boldsymbol{e}\|_{\epsilon,\Omega}\leq 2M_1\|\boldsymbol{F}(\boldsymbol{u}_h)\|_{-\epsilon,\Omega}. \qquad (22)$$

This proves the inequality (16). □

To build the relationship between $\boldsymbol{F}(\boldsymbol{u}_h)$ and the a posteriori error estimator η, some notations are given as follows. For a regular triangle partition $\mathcal{T}_h$ of Ω, $\mathcal{N}_h$ represents the set of all vertices divided in Ω, $\mathcal{E}_h$ represents all edges contained in $\mathcal{T}_h$, and $\mathcal{I}_h=\mathcal{E}_h\backslash\partial\Omega$ contains the inner edges of $\mathcal{T}_h$. We set $\widetilde{w}_T=\bigcup_{T\cap T'\neq\varnothing}T'$, $w_E=\bigcup_{E\in\partial T'}T'$, and $\widetilde{w}_E=\bigcup_{T'\in w_E}\bigcup_{T''\cap T'\neq\varnothing}T''$. $h_B=\mathrm{diam}(B)$ denotes the diameter of any set B. Let E be the shared edge of T and $\tilde{T}$, i.e., $E=T\cap\tilde{T}$, and $\boldsymbol{n}_E$ represent the outward normal vector of E in T, we define the jump across the edge by

$$[\nabla v\cdot\boldsymbol{n}_E]:=\nabla v\cdot\boldsymbol{n}_E|_T-\nabla v\cdot\boldsymbol{n}_E|_{\tilde{T}},\quad \forall v\in H_0^1(\Omega), \qquad (23)$$

and $\forall E\in\partial\Omega$, we set $[\nabla v\cdot\boldsymbol{n}_E]=0$ for convenience.

Next, we define $\widetilde{\boldsymbol{F}}(\boldsymbol{u}_h)$ by, $\forall\boldsymbol{v}=(v_1,v_2,v_3)\in(H_0^1(\Omega))^3$,

$$\begin{aligned}
&<\widetilde{\boldsymbol{F}}(\boldsymbol{u}_h),\boldsymbol{v}>\\
=\ &\int_\Omega(\nabla p_h\cdot\nabla v_1+p_h\nabla\psi_h\cdot\nabla v_1+\nabla n_h\cdot\nabla v_2-n_h\nabla\psi_h\cdot\nabla v_2\\
&+\epsilon\nabla\psi_h\cdot\nabla v_3-p_hv_3+n_hv_3)d\boldsymbol{x}-\sum_{T\in\mathcal{T}_h}\int_T(f_{T,1}v_1+f_{T,2}v_2+f_{T,3}v_3)d\boldsymbol{x}, \qquad (24)
\end{aligned}$$

with the mean value of f_i over T being $f_{T,i}=\int_T f_i d\boldsymbol{x}/|T|$, $i=1,2,3$. Here, $|T|$ denotes the area of T.

Let $\lambda_{T,i}$ $(i=1,2,3)$ be the area coordinates of the reference element T, we define the bubble functions b_T and b_E as follows,

$$b_T(\boldsymbol{x})=\begin{cases}27\lambda_{T,1}\lambda_{T,2}\lambda_{T,3}, & \boldsymbol{x}\in T,\\ 0, & \boldsymbol{x}\in\Omega\backslash T,\end{cases} \qquad (25)$$

$$b_E(\boldsymbol{x})=\begin{cases}4\lambda_{T_1,j}\lambda_{T_1,k}, & \boldsymbol{x}\in T_1,\\ 4\lambda_{T_2,l}\lambda_{T_2,m}, & \boldsymbol{x}\in T_2,\\ 0, & \boldsymbol{x}\in\Omega\backslash w_E,\end{cases} \qquad (26)$$

where j and k are the indices of E's two vertexes associated with T_1 while l and m are those with T_2, and $w_E = T_1 \cup T_2$. The space of vector bubble functions is then denoted by $\widetilde{\boldsymbol{Y}}_h := (\widetilde{Y}_h^0)^3$ with $\widetilde{Y}_h^0 = \text{span}\{b_T u,\ b_E P w : \forall u \in \mathcal{P}_1(T),\ \forall w \in \mathcal{P}_1(E),\ \forall T \in \mathcal{T}_h,\ \forall E \in \mathcal{I}_h\}$. Here, $\mathcal{P}_1(T)$ and $\mathcal{P}_1(E)$ are spaces of linear polynomials on T and E respectively and $P : L^\infty(E) \to L^\infty(T)$ is a continuation operator.

Two lemmas are now given before showing Theorem 2.

Lemma 2 *(The estimation of Clément interpolation* [17, 59]*)*

Let R_h be the Clément interpolation operator for a regular partition, then, $\forall v \in H_0^1(\Omega)$,

$$\|v - R_h v\|_{L^2(T)} \le M_2 h_T \|v\|_{1,\widetilde{w}_T}, \quad \forall T \in \mathcal{T}_h, \tag{27}$$

$$\|v - R_h v\|_{L^2(E)} \le M_3 h_E^{1/2} \|v\|_{1,\widetilde{w}_E}, \quad \forall E \in \mathcal{E}_h, \tag{28}$$

$$\|v - R_h v\|_{L^2(T)} \le M_4 \alpha_T \|v\|_{\epsilon,\widetilde{w}_T}, \quad \forall T \in \mathcal{T}_h, \tag{29}$$

$$\|v - R_h v\|_{L^2(E)} \le M_5 \epsilon^{-1/4} \alpha_E^{1/2} \|v\|_{\epsilon,\widetilde{w}_E}, \quad \forall E \in \mathcal{E}_h, \tag{30}$$

where $\alpha_S = \min\{1, h_S \epsilon^{-1/2}\}$ and S represent the edge E or element T. The constants M_2, ..., M_5 only depend on the reference element and regular partition.

Proof Inequalities (27) and (28) can be found in [17] and [59]. The main steps for the proof of inequalities (29) and (30) are briefly stated as following.

According to the definition of the *Clément* interpolation operator, we have

$$\|v - R_h v\|_{L^2(T)} \lesssim \|v\|_{L^2(\widetilde{w}_T)} \lesssim \|v\|_{\epsilon,\widetilde{w}_T},$$

and

$$\|v - R_h v\|_{L^2(T)} \lesssim h_T |v|_{1,\widetilde{w}_T} \lesssim h_T \epsilon^{-1/2} \|v\|_{\epsilon,\widetilde{w}_T},$$

which lead to inequality (29).

Additionally, we have

$$\begin{aligned}
&\|v - R_h v\|_{L^2(E)} \\
&\le \sum_{i=1}^{2} \|\lambda_i (v - R_h v)\|_{0,E} \\
&\lesssim h_{T'}^{-1/2} \|v - R_h v\|_{L^2(T')} + \|v - R_h v\|_{L^2(T')}^{1/2} \|\nabla (v - R_h v)\|_{L^2(T')}^{1/2} \\
&\lesssim h_{T'}^{-1/2} \alpha_{T'} \|v\|_{\epsilon,\widetilde{w}_{T'}} + \alpha_{T'}^{1/2} \|v\|_{\epsilon,\widetilde{w}_{T'}}^{1/2} |v|_{1,\widetilde{w}_{T'}}^{1/2} \\
&\lesssim h_{T'}^{-1/2} \alpha_{T'} \|v\|_{\epsilon,\widetilde{w}_{T'}} + \alpha_{T'}^{1/2} \epsilon^{-1/4} \|v\|_{\epsilon,\widetilde{w}_{T'}} \\
&\lesssim \epsilon^{-1/4} \alpha_{T'}^{1/2} \|v\|_{\epsilon,\widetilde{w}_{T'}},
\end{aligned} \tag{31}$$

where λ_i $(i = 1, 2)$ is the area coordinate corresponding to the two vertexes of E and $T' \in w_E$. This proves the inequality (30). The second inequality in (31) is based on trace inequality and scaling techniques. □

Lemma 3 *(Bubble function space [3, 57]) $\forall u \in \mathcal{P}_1(T)$ and $\forall w \in \mathcal{P}_1(E)$ where $T \in \mathcal{T}_h$ and $E \in \mathcal{I}_h$,*

$$v\widetilde{C}_1\|u\|_{L^2(T)} \le \|b_T u\|_{L^2(T)} \le \|u\|_{L^2(T)} \tag{32}$$

$$\widetilde{C}_2\|u\|_{L^2(T)} \le \sup_{v\in\mathcal{P}_1(T)} \frac{\int_T u b_T v d\boldsymbol{x}}{\|v\|_{L^2(T)}} \le \|u\|_{L^2(T)}, \tag{33}$$

$$\widetilde{C}_3\|w\|_{L^2(E)} \le \sup_{\tau\in\mathcal{P}_1(E)} \frac{\int_E w b_E P\tau ds}{\|\tau\|_{L^2(E)}} \le \|w\|_{L^2(E)}, \tag{34}$$

$$\widetilde{C}_4 h_T^{-1}\|u\|_{L^2(T)} \le \|\nabla(b_T u)\|_{L^2(T)} \le \widetilde{C}_5 h_T^{-1}\|u\|_{L^2(T)}, \tag{35}$$

$$\widetilde{C}_6 h_T^{-1}\|b_E P w\|_{L^2(T)} \le \|\nabla(b_E P w)\|_{L^2(T)} \le \widetilde{C}_7 h_T^{-1}\|b_E P w\|_{L^2(T)}, \tag{36}$$

$$\|\nabla(b_T u)\|_{L^2(T)} \le \widetilde{C}_8 h_T^{-1}\|u\|_{L^2(T)}, \tag{37}$$

$$\|b_E P w\|_{L^2(T)} \le \widetilde{C}_9 h_T^{1/2}\|w\|_{L^2(E)}, \tag{38}$$

$$\widetilde{C}_{10}\|u\|_{L^2(T)} \le \|b_T^{1/2} u\|_{L^2(T)} \le \|u\|_{L^2(T)}, \tag{39}$$

$$\widetilde{C}_{11}\|u\|_{L^2(E)} \le \|b_E^{1/2} P u\|_{L^2(T)} \le \|u\|_{L^2(E)}. \tag{40}$$

where the constants $\widetilde{C}_1, ..., \widetilde{C}_{11}$ depend on the reference element and regular partition only.

Theorem 2 *There exists a constant M_6 depending on the reference element and regular partition only, such that,*

$$\|\boldsymbol{F}(\boldsymbol{u}_h)\|_{-\epsilon,\Omega} \le M_6(\eta + \varepsilon), \tag{41}$$

where the estimator $\eta := \left(\sum_{T\in\mathcal{T}_h} \eta_T^2 + \sum_{E\in\mathcal{I}_h} \eta_E^2\right)^{1/2}$ and the oscillation term $\varepsilon := \left(\sum_{T\in\mathcal{T}_h} \varepsilon_T^2\right)^{1/2}$, with

$$\begin{aligned}
\eta_T^2 &:= h_T^2||\nabla\cdot(p_h\nabla\psi_h) + f_{T,1}||_{L^2(T)}^2 + h_T^2||\nabla\cdot(n_h\nabla\psi_h) - f_{T,2}||_{L^2(T)}^2 \\
&\quad + \alpha_T^2||n_h - p_h - f_{T,3}||_{L^2(T)}^2, \\
\eta_E^2 &:= h_E||[\nabla p_h\cdot\boldsymbol{n}_E] + [p_h\nabla\psi_h\cdot\boldsymbol{n}_E]\,||_{L^2(E)}^2 + h_E||[\nabla n_h\cdot\boldsymbol{n}_E] \\
&\quad - [n_h\nabla\psi_h\cdot\boldsymbol{n}_E]||_{L^2(E)}^2 + \epsilon^{-1/2}\alpha_E||\epsilon[\nabla\psi_h\cdot\boldsymbol{n}_E]||_{L^2(E)}^2\Big), \\
&:= h_T^2\sum_{i=1}^{2}||f_i - f_{T,i}||_{L^2(T)}^2 + \alpha_T^2||f_3 - f_{T,3}||_{L^2(T)}^2.
\end{aligned}$$

Proof We define $\boldsymbol{R}_h\boldsymbol{\phi} := (R_h\phi_1, R_h\phi_2, R_h\phi_3)$, $\forall\boldsymbol{\phi} = (\phi_1,\phi_2,\phi_3) \in (H_0^1(\Omega))^3$, with R_h a *Clemént* interpolation and have $\boldsymbol{R}_h \in \mathcal{L}((H_0^1(\Omega))^3, (V_h)^3)$. With $\boldsymbol{Y} = (H_0^1(\Omega))^3$, we denote by $\boldsymbol{Y}_h^*$ and $(\mathrm{Id}_{\boldsymbol{Y}} - \boldsymbol{R}_h)^*$ the dual spaces of $\boldsymbol{Y}_h = (V_h)^3$ and the

dual operator of $(\mathrm{Id}_{\boldsymbol{Y}} - \boldsymbol{R}_h)$, respectively. $\mathcal{L}(\boldsymbol{Y}, \boldsymbol{Y}_h)$ is a Banach space of continuous linear maps of $\boldsymbol{Y}$ in $\boldsymbol{Y}_h$.

Let $\boldsymbol{v}_h = \boldsymbol{R}_h\boldsymbol{\phi}$ in Eq. (8), thus,

$$\begin{aligned} & < \boldsymbol{F}(\boldsymbol{u}_h), \boldsymbol{\phi} > \\ = & < \boldsymbol{F}(\boldsymbol{u}_h), \boldsymbol{\phi} - \boldsymbol{R}_h\boldsymbol{\phi} > \\ = & < \widetilde{\boldsymbol{F}}(\boldsymbol{u}_h), \boldsymbol{\phi} - \boldsymbol{R}_h\boldsymbol{\phi} > + < \boldsymbol{F}(\boldsymbol{u}_h) - \widetilde{\boldsymbol{F}}(\boldsymbol{u}_h), \boldsymbol{\phi} - \boldsymbol{R}_h\boldsymbol{\phi} >, \end{aligned} \tag{42}$$

and,

$$\begin{aligned} & \|\boldsymbol{F}(\boldsymbol{u}_h)\|_{-\epsilon,\Omega} \\ \leq & \ \|(\mathrm{Id}_{\boldsymbol{Y}} - \boldsymbol{R}_h)^*\widetilde{\boldsymbol{F}}(\boldsymbol{u}_h)\|_{-\epsilon,\Omega} + \|(\mathrm{Id}_{\boldsymbol{Y}} - \boldsymbol{R}_h)^*(\boldsymbol{F}(\boldsymbol{u}_h) - \widetilde{\boldsymbol{F}}(\boldsymbol{u}_h))\|_{-\epsilon,\Omega}, \end{aligned} \tag{43}$$

with the two terms on the right-hand side (RHS) of the above inequality being discussed one by one in the following.

The first one is

$$\begin{aligned} & \| \ (\boldsymbol{Id}_{\boldsymbol{Y}} - \boldsymbol{R}_{\boldsymbol{h}})^*\widetilde{\boldsymbol{F}}(\boldsymbol{u}_h) \ \|_{-\epsilon,\Omega} \\ = & \sup_{\boldsymbol{\phi}\in\boldsymbol{Y}, \|\boldsymbol{\phi}\|_{\epsilon,\Omega}=1} \Big| \sum_{T\in\mathcal{T}_h} \Big\{ \int_T [(-\Delta p_h - \nabla\cdot(p_h\nabla\psi_h) - f_{T,1})(\phi_1 - R_h\phi_1) \\ & +(-\Delta n_h + \nabla\cdot(n_h\nabla\psi_h) - f_{T,2})(\phi_2 - R_h\phi_2) \\ & +(-\Delta\psi_h - p_h + n_h - f_{T,3})(\phi_3 - R_h\phi_3)]dx \\ & + \sum_{E\in\mathcal{I}_h\cap\partial T} \int_E [([\nabla p_h\cdot n_E] + [p_h\nabla\psi_h\cdot\boldsymbol{n}_E])(\phi_1 - R_h\phi_1) \\ & +([\nabla n_h\cdot\boldsymbol{n}_E] - [n_h\nabla\psi_h\cdot\boldsymbol{n}_E])(\phi_2 - R_h\phi_2) + \epsilon[\nabla\psi_h\cdot\boldsymbol{n}_E](\phi_3 - R_h\phi_3)]ds \Big\} \Big| \\ \lesssim & \sup_{\boldsymbol{\phi}\in\boldsymbol{Y}, \|\boldsymbol{\phi}\|_{\epsilon,\Omega}=1} \Big\{ \sum_{T\in\mathcal{T}_h} h_T(\| \ \nabla\cdot(p_h\nabla\psi_h) + f_{T,1} \ \|_{L^2(T)} \ \|\phi_1\|_{1,\widetilde{w}_T} \\ & + \| \ \nabla\cdot(n_h\nabla\psi_h) - f_{T,2} \ \|_{L^2(T)} \ \|\phi_2\|_{1,\widetilde{w}_T}) \\ & +\alpha_T \ \| \ n_h - p_h - f_{T,3} \ \|_{L^2(T)} \ \|\phi_3\|_{\epsilon,\widetilde{w}_T} \\ & + \sum_{E\in\mathcal{I}_h} h_E^{1/2}(\| \ [\nabla p_h\cdot\boldsymbol{n}_E] + [p_h\nabla\psi_h\cdot\boldsymbol{n}_E] \ \|_{L^2(E)}\|\phi_1\|_{1,\widetilde{w}_E} \\ & + \| \ [\nabla n_h\cdot\boldsymbol{n}_E] - [n_h\nabla\psi_h\cdot\boldsymbol{n}_E] \ \|_{L^2(E)} \ \|\phi_2\|_{1,\widetilde{w}_E}) \\ & +\epsilon^{-1/4}\alpha_E^{1/2} \ \| \ \epsilon[\nabla\psi_h\cdot\boldsymbol{n}_E] \ \|_{L^2(E)} \ \|\phi_3\|_{\epsilon,\widetilde{w}_E}) \Big\} \\ \lesssim & \sup_{\boldsymbol{\phi}\in\boldsymbol{Y}, \|\boldsymbol{\phi}\|_{\epsilon,\Omega}=1} \Big\{ \sum_{T\in\mathcal{T}_h} \eta_T(\|\phi_1\|^2_{1,\widetilde{w}_E} + \|\phi_2\|^2_{1,\widetilde{w}_E} + \|\phi_3\|^2_{\epsilon,\widetilde{w}_E})^{1/2} \\ & + \sum_{E\in\mathcal{I}_h} \eta_E(\|\phi_1\|^2_{1,\widetilde{w}_E} + \|\phi_2\|^2_{1,\widetilde{w}_E} + \|\phi_3\|^2_{\epsilon,\widetilde{w}_E})^{1/2} \Big\} \\ \lesssim & \ \eta, \end{aligned} \tag{44}$$

where the first inequality here is shown by combining inner edges of any triangle T and using inequalities (27) and (28). Cauchy-Schwartz inequality is utilized for giving the second and final inequalities.

Similarly, the second term on the RHS of (43) is

$$\begin{aligned}
&\|(\boldsymbol{Id}_{\boldsymbol{Y}} - \boldsymbol{R_h})^*[\boldsymbol{F}(\boldsymbol{u}_h) - \widetilde{\boldsymbol{F}}(\boldsymbol{u}_h)]\|_{-\epsilon,\Omega} \\
&\sup_{\boldsymbol{\phi}\in\boldsymbol{Y},\|\boldsymbol{\phi}\|_{\epsilon,\Omega}=1} \Big| \sum_{T\in\mathcal{T}_h} \int_T [(f_1 - f_{T,1})(\phi_1 - R_h\phi_1) + (f_2 - f_{T,2})(\phi_2 - R_h\phi_2) \\
&+(f_3 - f_{T,3})(\phi_3 - R_h\phi_3)]dx \Big| \\
\lesssim &\sup_{\boldsymbol{\phi}\in\boldsymbol{Y},\|\boldsymbol{\phi}\|_{\epsilon,\Omega}=1} \sum_{T\in\mathcal{T}_h} \Big(h_T\|f_1 - f_{T,1}\|_{L^2(T)}\|\phi_1\|_{1,\widetilde{w}_T} \\
&+h_T\|f_2 - f_{T,2}\|_{L^2(T)}\|\phi_2\|_{1,\widetilde{w}_T} + \alpha_T\|f_3 - f_{T,3}\|_{L^2(T)}\|\phi_3\|_{\epsilon,\widetilde{w}_T} \Big) \\
\lesssim &\ \varepsilon. \qquad (45)
\end{aligned}$$

Therefore, the results with two terms lead to the conclusion

$$\|\boldsymbol{F}(\boldsymbol{u}_h)\|_{-\epsilon,\Omega} \le M_6(\eta + \varepsilon), \qquad (46)$$

with M_6 independent of $\boldsymbol{u}_h$,$\boldsymbol{f}$ and ϵ. □

Similarly to the analysis in inequalities (20) and (21),

$$\begin{aligned}
\|\boldsymbol{e}\|_{1,\Omega} &\le M_1\|\widetilde{\boldsymbol{R}}\|_{-1,\Omega} \le \sqrt{2}M_1\|\nabla e_3\|_{L^\infty(\Omega)}\|\boldsymbol{e}\|_{1,\Omega} + \|\boldsymbol{F}(\boldsymbol{u}_h)\|_{-1,\Omega} \\
&\le \sqrt{2}M_1\|\nabla e_3\|_{L^\infty(\Omega)}\|\boldsymbol{e}\|_{1,\Omega} + \|\boldsymbol{F}(\boldsymbol{u}_h)\|_{-\epsilon,\Omega}. \qquad (47)
\end{aligned}$$

With Theorems 1 and 2, the following a posteriori error estimate is yielded for the equation system (2).

Theorem 3 *If p, n and $\boldsymbol{e}$ satisfy the conditions in Thm. 1, then*

$$\|\boldsymbol{e}\|_{\epsilon,\Omega} \le M_7(\eta + \varepsilon), \qquad (48)$$

$$\|\boldsymbol{e}\|_{*,\Omega} \le M_8(\eta + \varepsilon), \qquad (49)$$

where the constants M_7 and M_8 depend on the exact solution of (2) but are independent of $\boldsymbol{e}$, $\boldsymbol{u}_h$, ϵ and the mesh size.

3.2 Lower bounds of the error

The special bubble function is defined before showing the lower bound in Theorem 4. Given any number $\mu \in (0, 1]$, we denote by $F_\mu : R^2 \to R^2$ the transformation which maps $\boldsymbol{x} = (x, y)$ on $(\mu x, y)$. Let $B_\mu = diag(\mu, 1)$, $F_\mu(\boldsymbol{x}) = B_\mu\boldsymbol{x}^\tau$. $\forall T \in \mathcal{T}_h$ we set invertible affine map on reference element $\hat{T}$ that $F_T(\hat{x}, \hat{y}) = B_T(\hat{x}, \hat{y})^\tau + \boldsymbol{b} = \boldsymbol{x}^\tau \in T$, $\forall(\hat{x}, \hat{y}) \in \hat{T}$.

According to the above definitions about the transformations of coordinates, we have the bubble function $b_{\hat{E}} = b_{\hat{E}}(\hat{x}, \hat{y}) = b_{\hat{E}}(F_\mu^{-1}(\mu\hat{x}, \hat{y})) = b_{\hat{E}} \circ F_\mu^{-1}(\mu\hat{x}, \hat{y}) \doteq b_{\hat{E},\mu}$ for any $(\hat{x}, \hat{y}) \in \hat{E}$, where $b_{\hat{E},\mu}$ is the edge bubble function on $\hat{T}_\mu$ and $\hat{T}_\mu =$

$F_\mu(\hat{T})$. We set $b_{\hat{E},\mu} = 0$ on $\hat{T} \setminus \hat{T}_\mu$ for simplicity and define the function on $w_E = T_1 \cup T_2$ with $w \in H^1(E)$ as follows.

$$b_{E,\mu} w(\boldsymbol{x}) = \begin{cases} b_{E,\mu_1} P w, & \boldsymbol{x} \in T_1, \\ b_{E,\mu_2} P w, & \boldsymbol{x} \in T_2, \end{cases} \tag{50}$$

and $b_{E,\mu_1}|_E = b_{E,\mu_2}|_E = b_E|_E$.

Lemma 4 *(Special bubble function [59]) For any $T \in \mathcal{T}_h$, E is one of its edge, then $\forall w \in P_1(E)$,*

$$\|b_{E,\mu} P w\|_{L^2(T)} \le M_9 h_E^{1/2} \mu^{1/2} \|w\|_E, \tag{51}$$

$$\|\nabla(b_{E,\mu} P w)\|_{L^2(T)} \le M_{10} h_E^{-1/2} \mu^{-1/2} \|w\|_E, \tag{52}$$

where the constants M_9 and M_{10} depend on the reference element and regular partition only.

Proof On the reference element $\hat{T}$,

$$\begin{aligned} \|b_{\hat{E},\mu} P \hat{w}\|_{L^2(\hat{T})} &= \|b_{\hat{E},\mu} P \hat{w}\|_{L^2(\hat{T}_\mu)} \lesssim |det\, B_\mu|^{1/2} \|b_{\hat{E}} P \hat{w}\|_{L^2(\hat{T})} \\ &\lesssim |det\, B_\mu|^{1/2} h_{\hat{E}}^{1/2} \|\hat{w}\|_{L^2(\hat{E})} \lesssim \mu^{1/2} \|\hat{w}\|_{L^2(\hat{E})}, \end{aligned} \tag{53}$$

and

$$\begin{aligned} \|\hat{\nabla}(b_{\hat{E},\mu} P \hat{w})\|_{L^2(\hat{T})} &= \|\hat{\nabla}(b_{\hat{E},\mu} P \hat{w})\|_{L^2(\hat{T}_\mu)} \lesssim |det\, B_\mu|^{1/2} \|B_\mu^{-T}\| \|\hat{\nabla}(b_{\hat{E}} P \hat{w})\|_{L^2(\hat{T})} \\ &\lesssim \mu^{1/2} \mu^{-1} \|\hat{w}\|_{L^2(\hat{E})} \\ &\lesssim \mu^{-1/2} \|\hat{w}\|_{L^2(\hat{E})}. \end{aligned} \tag{54}$$

Based on the scaling techniques and the regularity of T, inequalities (51) and (52) are proved. □

Theorem 4 *There exist constants M_{11} and M_{12} depending on the reference element and regular partition only, such that*

$$\eta_T \le M_{11} \Big(\sup_{\boldsymbol{v} \in \widetilde{\boldsymbol{Y}}_h|_T, \|\boldsymbol{v}\|_{*,T}=1} | < \widetilde{\boldsymbol{F}}(\boldsymbol{u}_h), \boldsymbol{v} >_T | + \|\boldsymbol{e}\|_{\epsilon,T} + \varepsilon_T \Big), \quad \forall T \in \mathcal{T}_h, \tag{55}$$

and

$$\eta_E \le M_{12} \Big(\sup_{\boldsymbol{v} \in \widetilde{\boldsymbol{Y}}_h|_T, \|\boldsymbol{v}\|_{*,T}=1} | < \widetilde{\boldsymbol{F}}(\boldsymbol{u}_h), \boldsymbol{v} >_T | + \|\boldsymbol{e}\|_{\epsilon,w_E} + \varepsilon_{w_E} \Big), \quad \forall E \in \mathcal{I}_h, \tag{56}$$

where $\varepsilon_{w_E} := \left(\sum_{T \in w_E} \varepsilon_T^2 \right)^{1/2}$.

Proof The inequality with η_T is considered first, i.e., we have

$$\begin{aligned}
& h_T||\nabla\cdot(p_h\nabla\psi_h)+f_{T,1}||_{L^2(T)}\\
=\ & h_T\|\Delta p_h+\nabla\cdot(p_h\nabla\psi_h)+f_{T,1}\|_{L^2(T)}\\
\lesssim\ & h_T\sup_{\phi\in\mathcal{P}_1(T)\setminus\{0\}}|<\Delta p_h+\nabla\cdot(p_h\nabla\psi_h)+f_{T,1},b_T\phi>_T|\cdot\|\phi\|^{-1}_{L^2(T)}\\
\lesssim\ & \sup_{\phi\in\mathcal{P}_1(T)\setminus\{0\}}|<\Delta p_h+\nabla\cdot(p_h\nabla\psi_h)+f_{T,1},b_T\phi>_T|\cdot|b_T\phi|^{-1}_{1,T}\\
\lesssim\ & \sup_{\phi\in\mathcal{P}_1(T)\setminus\{0\},\|b_T\phi\|_{1,T}=1}|<\widetilde{\boldsymbol{F}}(\boldsymbol{u}_h),(b_T\phi,0,0)>_T|\\
\lesssim\ & \sup_{\boldsymbol{v}\in\widetilde{\boldsymbol{Y}}_h|_T,\|\boldsymbol{v}\|_{*,T}=1}|<\widetilde{\boldsymbol{F}}(\boldsymbol{u}_h),\boldsymbol{v}>_T|,
\end{aligned}\tag{57}$$

where (33) is applied for obtaining the first inequality, and inequalities (32) and (35) are used for getting the second inequality.

Analogously, we have

$$h_T\|\nabla\cdot(n_h\nabla\psi_h)-f_{T,2}\|_{L^2(T)}\lesssim\sup_{\boldsymbol{v}\in\widetilde{\boldsymbol{Y}}_h|_T,\|\boldsymbol{v}\|_{*,T}=1}|<\widetilde{\boldsymbol{F}}(\boldsymbol{u}_h),\boldsymbol{v}>_T|.\tag{58}$$

Denoting $y:=b_T(n_h-p_h-f_{T,3})$, we have

$$\begin{aligned}
& \|b_T^{1/2}(n_h-p_h-f_{T,3})\|^2_{L^2(T)}\\
=\ & \int_T[(n_h-n)y-(p_h-p)y-\epsilon\nabla(\psi-\psi_h)\cdot\nabla y]d\boldsymbol{x}+\int_T(f_3-f_{T,3})yd\boldsymbol{x}\\
\le\ & \|n_h-n\|_{L^2(T)}\|y\|_{L^2(T)}+\|p_h-p\|_{L^2(T)}\|y\|_{L^2(T)}\\
& +\epsilon\|\nabla(\psi_h-\psi)\|_{L^2(T)}\|\nabla y\|_{L^2(T)}+\|f_3-f_{T,3}\|_{L^2(T)}\|y\|_{L^2(T)}\\
\le\ & (\|n_h-n\|_{L^2(T)}+\|f_3-f_{T,3}\|_{L^2(T)}+\|p_h-p\|_{L^2(T)})\|n_h-p_h-f_{T,3}\|_{L^2(T)}\\
& +\epsilon h_T^{-1}\|\nabla(\psi_h-\psi)\|_{L^2(T)}\|n_h-p_h-f_{T,3}\|_{L^2(T)},
\end{aligned}$$

where the last inequality is obtained by inequalities (32) and (37). Together with the inequality (39) and $\alpha_T\epsilon h_T^{-1}\le\epsilon^{1/2}$, it reads

$$\begin{aligned}
& \alpha_T\|n_h-p_h-f_{T,3}\|_{L^2(T)}\\
\lesssim\ & \|n_h-n\|_{L^2(T)}+\alpha_T\|f_3-f_{T,3}\|_{L^2(T)}+\|p_h-p\|_{L^2(T)}+\epsilon^{1/2}\|\nabla(\psi_h-\psi)\|_{L^2(T)}\\
\lesssim\ & \|\boldsymbol{e}\|_{\epsilon,T}+\alpha_T\|f_3-f_{T,3}\|_{L^2(T)}.
\end{aligned}\tag{59}$$

Thus, the inequality (55) is proved with the definition of η_T and ε_T.

On the side of η_E, $\forall E\in\mathcal{I}_h$, we have

$$\begin{aligned}
& h_E^{1/2}||[\nabla p_h\cdot\boldsymbol{n}_E]+[p_h\nabla\psi_h\cdot\boldsymbol{n}_E]||_{L^2(E)}\\
\lesssim\ & h_E^{1/2}\sup_{\delta\in\mathcal{P}_1(E)\setminus\{0\}}||\delta||^{-1}_{L^2(E)}\left|\int_E([\nabla p_h\cdot\boldsymbol{n}_E]+[p_h\nabla\psi_h\cdot\boldsymbol{n}_E])b_EP\delta ds\right|\\
\lesssim\ & h_E^{1/2}h_T^{1/2}\sup_{\delta\in\mathcal{P}_1(E)\setminus\{0\}}||b_EP\delta||^{-1}_{L^2(T)}\left|\int_E([\nabla p_h\cdot\boldsymbol{n}_E]+[p_h\nabla\psi_h\cdot\boldsymbol{n}_E])b_EP\delta ds\right|
\end{aligned}$$

$$
\begin{aligned}
&\lesssim h_T \sup_{\delta\in\mathcal{P}_1(E)\setminus\{0\}} ||b_E P\delta||^{-1}_{L^2(T)} \Big| < \widetilde{\boldsymbol{F}}(\boldsymbol{u}_h), (b_E P\delta, 0, 0) >_{w_E} \\
&\quad - \int_{w_E} (-\Delta p_h - \nabla\cdot(p_h\nabla\psi_h) - f_{T,1}) b_E P\delta dx \Big| \\
&\lesssim \sum_{T\in w_E} \left[\sup_{\boldsymbol{v}\in\widetilde{\boldsymbol{Y}}_h|_T, \|\boldsymbol{v}\|_{*,T}=1} | < \widetilde{\boldsymbol{F}}(\boldsymbol{u}_h), \boldsymbol{v} >_T | + h_T ||\nabla\cdot(p_h\nabla\psi_h) + f_{T,1}||_{L^2(T)} \right] \\
&\lesssim \sum_{T\in w_E} \sup_{\boldsymbol{v}\in\widetilde{\boldsymbol{Y}}_h|_T, \|\boldsymbol{v}\|_{*,T}=1} | < \widetilde{\boldsymbol{F}}(\boldsymbol{u}_h), \boldsymbol{v} >_T |, \qquad (60)
\end{aligned}
$$

where h_T represents the maximal diameter of T in w_E. Inequalities (34) and (38) are applied for showing the first and second inequality, respectively, and (36) is used to have the fourth inequality here.

Similarly, we derive

$$
\begin{aligned}
&h_E^{1/2} ||[\nabla n_h\cdot\boldsymbol{n}_E] - [n_h\nabla\psi_h\cdot\boldsymbol{n}_E]||_{L^2(E)} \\
&\lesssim \sum_{T\in w_E} \sup_{\boldsymbol{v}\in\widetilde{\boldsymbol{Y}}_h|_T, \|\boldsymbol{v}\|_{*,T}=1} | < \widetilde{\boldsymbol{F}}(\boldsymbol{u}_h), \boldsymbol{v} >_T |. \qquad (61)
\end{aligned}
$$

Let $r = b_{E,\mu}\epsilon[\nabla\psi_h\cdot\boldsymbol{n}_E]$ with the constant μ to be determined later, with Green formulation, Lemma (4) we have

$$
\begin{aligned}
&\int_E (\epsilon[\nabla\psi_h\cdot\boldsymbol{n}_E]) r ds \\
&= \int_{w_E} \epsilon\nabla\psi_h\cdot\nabla r d\boldsymbol{x} \\
&= \int_{w_E} \epsilon\nabla(\psi_h-\psi)\cdot\nabla r d\boldsymbol{x} + \int_{w_E} (p-p_h) r d\boldsymbol{x} - \int_{w_E} (n-n_h) r d\boldsymbol{x} \\
&\quad + \sum_{T\in w_E} \left[\int_T (f_3 - f_{T,3}) r d\boldsymbol{x} - \int_T (p_h - n_h + f_{T,3}) r d\boldsymbol{x} \right] \\
&\quad \le \epsilon^{1/2}\|\nabla(\psi_h-\psi)\|_{L^2(w_E)} \epsilon^{1/2}\|\nabla r\|_{L^2(w_E)} + \Big(\|p-p_h\|_{L^2(w_E)} + \|n-n_h\|_{L^2(w_E)} \\
&\quad + \sum_{T\in w_E} \|f_3 - f_{T,3}\|_{L^2(T)} \Big) \|r\|_{L^2(w_E)} + \Big(\sum_{T\in w_E} \|n_h - p_h - f_{T,3}\|_{L^2(T)} \Big) \|r\|_{L^2(w_E)} \\
&\quad \lesssim \sum_{i=1}^{2} \Big[\epsilon^{1/2}\|\nabla(\psi_h-\psi)\|_{L^2(w_E)} \epsilon^{1/2} \mu_i^{-1/2} h_E^{-1/2} \|\epsilon[\nabla\psi_h\cdot\boldsymbol{n}_E]\|_{L^2(E)} \\
&\quad + \Big(\|p-p_h\|_{L^2(w_E)} + \|n-n_h\|_{L^2(w_E)} \\
&\quad + \sum_{T\in w_E} \|f_3 - f_{T,3}\|_{L^2(T)} \Big) h_E^{1/2} \mu_i^{1/2} \|\epsilon[\nabla\psi_h\cdot\boldsymbol{n}_E]\|_{L^2(E)} \\
&\quad + \sum_{T\in w_E} \|n_h - p_h - f_{T,3}\|_{L^2(T)} \mu_i^{1/2} h_E^{1/2} \|\epsilon[\nabla\psi_h\cdot\boldsymbol{n}_E]\|_{L^2(E)} \Big]. \qquad (62)
\end{aligned}
$$

We then choose $\mu_i = \epsilon^{1/2} h_E^{-1} \alpha_E < 1$ and have

$$\begin{aligned}
&\epsilon^{-1/4} \alpha_E^{1/2} \|\epsilon[\nabla \psi_h \cdot \boldsymbol{n}_E]\|_{L^2(E)} \\
\lesssim\ & \epsilon^{1/2} \|\nabla(\psi_h - \psi)\|_{L^2(w_E)} \epsilon^{1/4} + \Big[\|p - p_h\|_{L^2(w_E)} + \|n - n_h\|_{L^2(w_E)} \\
&+ \sum_{T \in w_E} (\|f_3 - f_{T,3}\|_{L^2(T)} + \|n_h - p_h - f_{T,3}\|_{L^2(T)}) \Big] \alpha_E \\
\lesssim\ & \|\boldsymbol{e}\|_{\epsilon, w_E} + \sum_{T \in w_E} \alpha_T \|f_3 - f_{T,3}\|_{L^2(T)}, \qquad (63)
\end{aligned}$$

where the regular mesh, inequalities (40) and (59) are used. Now, inequality (56) is proved with the definition of η_E and ε_T. □

Theorem 5 *If p, n and $\boldsymbol{e}$ satisfy the conditions in Thm. 1,*

$$\sup_{\boldsymbol{v} \in \widetilde{\boldsymbol{Y}}_h|_T, \|\boldsymbol{v}\|_{*,T}=1} | < \widetilde{\boldsymbol{F}}(\boldsymbol{u}_h), \boldsymbol{v} >_T | \le M_{14}(\|\boldsymbol{e}\|_{*,T} + \rho_T), \qquad (64)$$

where $\rho_T^2 := h_T^2 \sum_{i=1}^{3} \|f_i - f_{T,i}\|^2_{L^2(T)}$, and M_{14} depends on the exact solution of (2) but is independent of $\boldsymbol{u}_h$, $\boldsymbol{f}$, ϵ and the mesh size.

Proof We rewrite inequalities (14) and (18) as

$$| < \boldsymbol{DF}(\boldsymbol{u})\boldsymbol{\phi}, \boldsymbol{v} > | \lesssim \|\boldsymbol{\phi}\|_{\epsilon,T} \|\boldsymbol{v}\|_{\epsilon,T} + \|\boldsymbol{\phi}\|_{1,T} \|\boldsymbol{v}\|_{1,T} \le M_{13} \|\boldsymbol{\phi}\|_{*,T} \|\boldsymbol{v}\|_{*,T}, \qquad (65)$$

and

$$< \boldsymbol{F}(\boldsymbol{u}_h), \boldsymbol{w} > = < \boldsymbol{DF}(\boldsymbol{u})\boldsymbol{e}, \boldsymbol{w} > - \int_0^1 < \boldsymbol{DF}(\boldsymbol{u})\boldsymbol{e} - \boldsymbol{DF}(\boldsymbol{u} + t\boldsymbol{e})\boldsymbol{e}, \boldsymbol{w} > dt. \qquad (66)$$

When $\|\nabla e_3\|_{L^\infty(\Omega)} \le 1/(2\sqrt{2}M_1)$,

$$\begin{aligned}
\sup_{\boldsymbol{v} \in \widetilde{\boldsymbol{Y}}_h|_T, \|\boldsymbol{v}\|_{*,T}=1} | < \boldsymbol{F}(\boldsymbol{u}_h), \boldsymbol{v} >_T | &\le M_{13} \|\boldsymbol{e}\|_{\epsilon,T} + \sqrt{2} \|\nabla e_3\|_{L^\infty(\Omega)} \|\boldsymbol{e}\|_{*,T} \\
&\le (1/(M_{13}) + 1/(2M_1)) \|\boldsymbol{e}\|_{*,T}. \qquad (67)
\end{aligned}$$

Then

$$\begin{aligned}
&\sup_{\boldsymbol{\delta} \in \widetilde{\boldsymbol{Y}}_h|_T, \|\boldsymbol{\delta}\|_{*,T}=1} | < \boldsymbol{F}(\boldsymbol{u}_h) - \widetilde{\boldsymbol{F}}(\boldsymbol{u}_h), \boldsymbol{\delta} > | \qquad (68) \\
=\ & \sup_{\boldsymbol{\delta} \in \widetilde{\boldsymbol{Y}}_h|_T, \|\boldsymbol{\delta}\|_{*,T}=1} \Big| \int_T [(f_1 - f_{T,1})\delta_1 + (f_2 - f_{T,2})\delta_2 + (f_3 - f_{T,3})\delta_3] dx \Big| \\
\lesssim\ & \sup_{\boldsymbol{\delta} \in \tilde{Y}_h|_T, \|\boldsymbol{\delta}\|_{*,T}=1} h_T \Big(\|f_1 - f_{T,1}\|_{L^2(T)} \|\delta_1\|_{1,T} + \|f_2 - f_{T,2}\|_{L^2(T)} \|\delta_2\|_{1,T} \\
&+ \|f_3 - f_{T,3}\|_{L^2(T)} \|\delta_3\|_{1,T} \Big) \\
\lesssim\ & \rho_T.
\end{aligned}$$

Here, $\boldsymbol{\delta} = (\delta_1, \delta_2, \delta_3)$. To prove the first inequality in (68), the following inequalities are used.

$$\|\delta_i\|_{L^2(T)} \lesssim \|b_T\delta_i\|_{L^2(T)} \lesssim h_T\|\nabla(b_T\delta_i)\|_{L^2(T)} \lesssim h_T\|\delta_i\|_{1,T},\ i = 1, 2, 3. \tag{69}$$

Furthermore,

$$\begin{aligned} &\sup_{\boldsymbol{v}\in\widetilde{\boldsymbol{Y}}_h|_T, \|\boldsymbol{v}\|_{*,T}=1} |< \widetilde{\boldsymbol{F}}(\boldsymbol{u}_h), \boldsymbol{v} >_T| \\ \le &\sup_{\boldsymbol{v}\in\widetilde{\boldsymbol{Y}}_h|_T, \|\boldsymbol{v}\|_{*,T}=1} |< \boldsymbol{F}(\boldsymbol{u}_h), \boldsymbol{v} >_T| \\ &+ \sup_{\boldsymbol{v}\in\widetilde{\boldsymbol{Y}}_h|_T, \|\boldsymbol{v}\|_{*,T}=1} |< \boldsymbol{F}(\boldsymbol{u}_h) - \widetilde{\boldsymbol{F}}(\boldsymbol{u}_h), \boldsymbol{v} >_T|, \end{aligned} \tag{70}$$

thus, inequality (64) is proved. □

According to the above analysis, we have the robust lower bound of error as follows.

Theorem 6 *If p, n and $\boldsymbol{e}$ satisfy the conditions in Thm. 1,*

$$\eta_T \le M_{15}(\|\boldsymbol{e}\|_{*,T} + \rho_T + \varepsilon_T), \quad \forall T \in \mathcal{T}_h, \tag{71}$$

and

$$\eta_E \le M_{16}(\|\boldsymbol{e}\|_{*,w_E} + \rho_{w_E} + \varepsilon_{w_E}), \quad \forall E \in \mathcal{I}_h, \tag{72}$$

where M_{15} and M_{16} depend on the exact solution of (2) but are independent of $\boldsymbol{e}$, $\boldsymbol{u}_h$, ϵ and the mesh size.

Remark 1 Together with the left inequality in (16) as taking the domain to be T, inequalities (71) and (72) lead to the conclusion that $\eta \lesssim \|\boldsymbol{e}\|_{*,\Omega} + \rho + \varepsilon$ where $\rho = (\sum_{T\in\mathcal{T}_h}\rho_T^2)^{1/2}$. On the other hand, inequality (49) gives $\|\boldsymbol{e}\|_{*,\Omega} \lesssim \eta + \varepsilon$. As f_i is piecewise H^s $(0 < s \le 1)$ over $\mathcal{T}_h$, the oscillation term $\rho = \mathcal{O}(h^{1+s})$ [50], i.e., a higher order term of $\|\boldsymbol{e}\|_{*,\Omega}$. Specifically, $\|f_i - f_{T,i}\|_{L^2(T)} \lesssim h\|f_i\|_{1,T}$, $\forall f_i \in H^1(T)$, and $\|f_i - f_{T,i}\|_{L^2(T)} = 0$ when f_i is a piecewise-constant function on $\mathcal{T}_h$. Thus, we have the desired result at the leading order as inequality (11) shows, i.e., $\underline{C}\eta \le \|\boldsymbol{e}\|_{*,\Omega} \le \overline{C}\eta$, with constants $\underline{C}$ and $\overline{C}$ independent of $\boldsymbol{e}$, $\boldsymbol{u}_h$, ϵ and the mesh size. However, more thorough discussions need to be done carefully for the general case with $f_i \in L^2(T)$.

4 Numerical experiments

During the numerical procedure, we involve the well-known cycle of the adaptive method, that is "*SOLVE* → *ESTIMATE* → *MARK* → *REFINE*." The details of the four steps are stated as follows.

SOLVE: An adaptive two-grid finite element method [39, 67] is applied to solve the nonlinear system, see pseudocode in Table 1. In the process of finite element discretizations, we use the edge-averaged finite element (EAFE) scheme in [64] which was discussed later in [8, 48] for the PNP system.

ESTIMATE: The a posteriori error estimator η introduced in Section 3 is applied to estimate the error.

MARK: The maximum marking strategy [12, 21] is utilized for remarking the grid.

REFINE: The newest vertex bisection method [6] is used to refine the marked grid. Simultaneously, the new grid is created.

We run the above loops to produce adaptive meshes until the criterion for the fixed maximal degree of freedom N is arrived, i.e., $N = \mathcal{O}(10^5)$. All examples are in two dimensions and simulations are performed with the finite element software IFEM. The first and second examples with $\epsilon = 1$ are aimed to validate the a posteriori error

Table 1 Algorithm of the two-grid method for solving the steady-state PNP equations

Algorithm 1 Solve the steady-state PNP equations

Let $\mathcal{T}_k$ be the kth level of grid in the adaptive cycle, $\boldsymbol{Y}_{h_k}$ be the corresponding finite element space, and $(p_{h_k}, n_{h_k}, \psi_{h_k})$ be the finite element solutions on $\mathcal{T}_k$, $k \geq 0$. $\mathcal{T}_0$ and $\mathcal{T}_1$ are given and $(p_{h_0}, n_{h_0}) = \mathbf{0}$.

Step 1: On the kth level of grid, $\mathcal{T}_k$.

Set $(p^{(0)}, n^{(0)}) = (p_{h_k}, n_{h_k})$.

(1) Run the iteration:

For $l \geq 0$, find $(p^{(l+1)}, n^{(l+1)}, \psi^{(l+1)})$ such that $\forall (v_{1,h_k}, v_{2,h_k}, v_{3,h_k}) \in \boldsymbol{Y}_{h_k}$,

$$(\nabla \psi^{(l+1)}, \nabla v_{3,h_k}) - (p^{(l)}, v_{3,h_k}) + (n^{(l)}, v_{3,h_k}) = (f_3, v_{3,h_k}),$$

and

$$\begin{cases} (\nabla p^{(l+1)}, \nabla v_{1,h_k}) + (p^{(l+1)} \nabla \psi^{(l+1)}, \nabla v_{1,h_k}) = (f_1, v_{1,h_k}), \\ (\nabla n^{(l+1)}, \nabla v_{2,h_k}) - (n^{(l+1)} \nabla \psi^{(l+1)}, \nabla v_{2,h_k}) = (f_2, v_{2,h_k}). \end{cases}$$

(2) Examine the stop criterion:

If $\|\psi^{(l+1)} - \psi^{(l)}\|_{L^2(\Omega)} < Tol$, (here we set $Tol = 10^{-5}$),

$(p_{h_k}, n_{h_k}, \psi_{h_k}) = (p^{(l+1)}, n^{(l+1)}, \psi^{(l+1)})$, break.

Else,

set $l \leftarrow l + 1$, continue with the iteration.

Step 2: Prolong the solution on the grid $\mathcal{T}_k$ to $\mathcal{T}_{k+1}$.

Construct the prolong operator based on $\mathcal{T}_k$ and $\mathcal{T}_{k+1}$[63].

Prolong $(p_{h_k}, n_{h_k}, \psi_{h_k})$ to grid $\mathcal{T}_{k+1}$, and set the prolong result as $(p_{pro}, n_{pro}, \psi_{pro})$.

Step 3: To find $(p_{h_{k+1}}, n_{h_{k+1}}, \psi_{h_{k+1}})$ such that $\forall (v_{1,h_{k+1}}, v_{2,h_{k+1}}, v_{3,h_{k+1}}) \in \boldsymbol{Y}_{h_{k+1}}$,

$$(\nabla \psi_{h_{k+1}}, \nabla v_{3,h_{k+1}}) - (p_{pro}, v_{3,h_{k+1}}) + (n_{pro}, v_{3,h_{k+1}}) = (f_3, v_{3,h_{k+1}}).;$$

and

$$\begin{cases} (\nabla p_{h_{k+1}}, \nabla v_{1,h_{k+1}}) + (p_{h_{k+1}} \nabla \psi_{pro}, \nabla v_{1,h_{k+1}}) = (f_1, v_{1,h_{k+1}}), \\ (\nabla n_{h_{k+1}}, \nabla v_{2,h_{k+1}}) - (n_{h_{k+1}} \nabla \psi_{pro}, \nabla v_{2,h_{k+1}}) = (f_2, v_{2,h_{k+1}}). \end{cases}$$

estimation theory and show the application of the adaptive method for geometrical singularities, respectively. The third example discusses the boundary layer effects with $\epsilon < 1$.

Example 1 We take

$$\begin{cases} p = \sin(2\pi x)\sin(2\pi y), \\ n = \sin(3\pi x)\sin(3\pi y), \\ \psi = \sin(\pi x)\sin(\pi y), \end{cases} \tag{73}$$

as an exact solution of the PNP equation system (2) with $\epsilon = 1$ in the L-shaped domain, $\Omega = [-1, 1] \times [-1, 1] \setminus [0, 1] \times [-1, 0]$, with homogeneous boundary conditions. Consequently, functions f_1, f_2 and f_3 on the RHS are determined by the exact solution.

The problem is solved by the adaptive algorithm and Fig. 1 shows the result with the degree of freedom $N = 951$ and the error $||\boldsymbol{e}||_{L^2(\Omega)} \sim 7 \times 10^{-2}$. Panels (a-c) show the numerical solutions of p, n and ψ, and panel (d) shows the corresponding adaptive mesh refinements. The nonuniform grids illustrate the fact that the a posteriori error estimate works here; nevertheless, we do not observe obvious adaptivity, which is caused by the fact that the synthetic solution we choose is sufficiently regular, i.e., the adaptive algorithm is not highly required for solving it efficiently.

Furthermore, we run the algorithm until $N = 2 \times 10^5$ and test the a posteriori error estimation theory by the exact solution. With N increased adaptively, the error analysis is shown in Fig. 2 where both H^1 and L^2 errors of the solution and the a posteriori error estimator η are presented. For $N > 10^2$, the H^1 and L^2 errors converge to $\mathcal{O}(N^{-1/2})$ and $\mathcal{O}(N^{-1})$, respectively, which are as expected for linear finite element interpolations. For large number of N, i.e., $N > 10^3$, η converges to $\mathcal{O}(N^{-1/2})$, embodying that the error of the numerical solution is well controlled by the a posteriori error estimator η of which the reliability and efficiency are hence numerically shown.

Example 2 In order to demonstrate the adaptive performance of the estimator η for geometrical singularities, we choose $f_1 = f_2 = f_3 = 1$ and rewrite the problem (2) with $\epsilon = 1$ as follows,

$$\begin{cases} -\Delta p - \nabla \cdot (p\nabla\psi) = 1, \\ -\Delta n + \nabla \cdot (n\nabla\psi) = 1, \\ -\Delta\psi - p + n = 1, \end{cases} \tag{74}$$

by which we need find $p(\boldsymbol{x}), n(\boldsymbol{x}), \psi(\boldsymbol{x}) \in H_0^1(\Omega)$ with the same computational domain as in Example 1.

To illustrate the adaptive mesh refinements clearly, we report the mesh grid for $N = 1243$ in Fig. 3 (panel (d)). The corresponding numerical results for p, n and ψ presented in panels (a, b, c) are quite smooth, however, it is evident to observe the adaptive mesh refinements near the corner point $(0, 0)$, which indicates the well performance of the a posteriori error estimator η proposed in current work. More specifically, we calculate the numerical value of the indicator η versus N and present

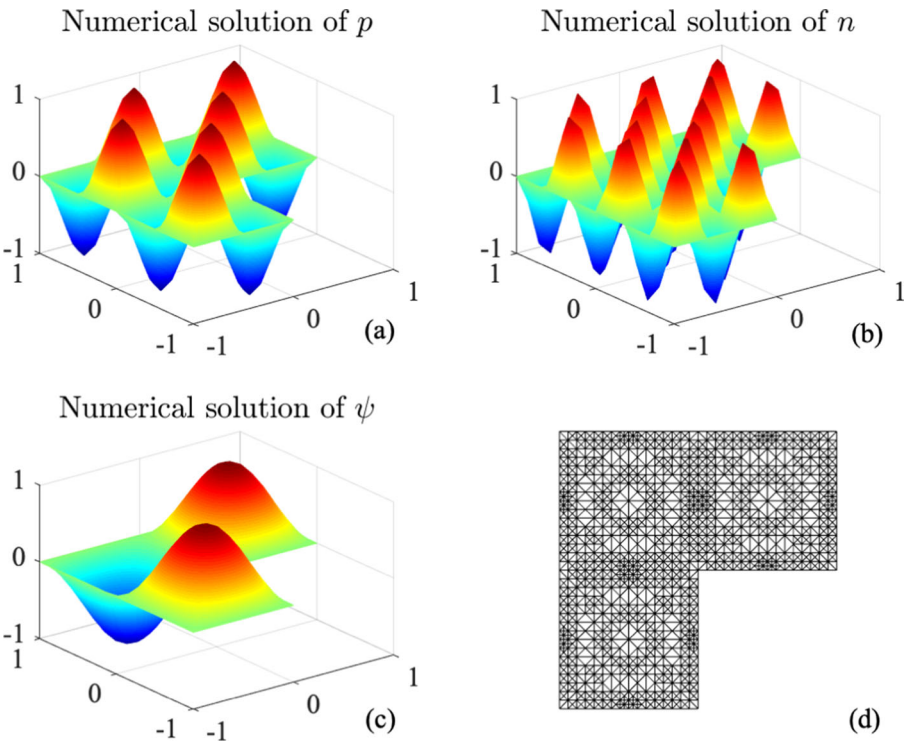

Fig. 1 The numerical solution of p, n, ψ (a, b, c), and the final mesh grid (d) for Example 1 with $N = 951$ and $||e||_{L^2(\Omega)} \sim 7 \times 10^{-2}$

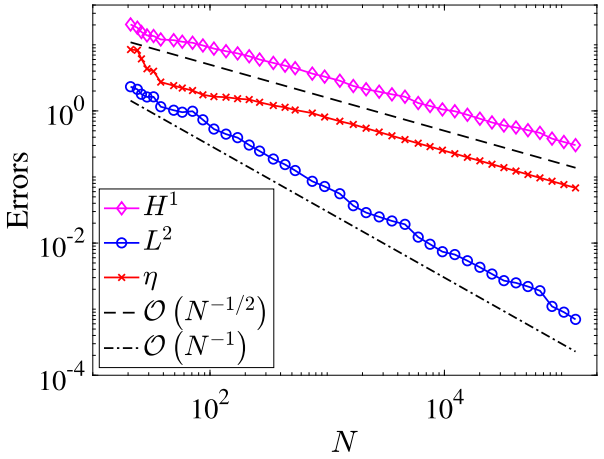

Fig. 2 The numerical errors are compared with analytical results. The H^1 error of the solution (diamond) and the a posteriori error estimator η (circle) both converge to $\mathcal{O}(N^{-1/2})$ for large N. The L^2 error of the solution (cross) converges to $\mathcal{O}(N^{-1})$

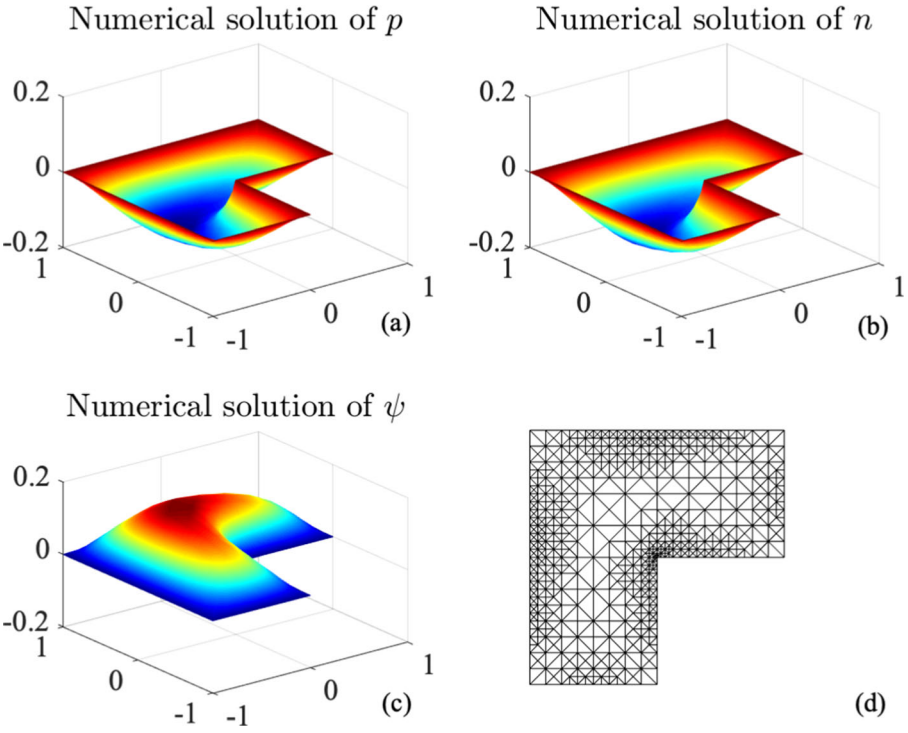

Fig. 3 The numerical solution of p, n and ψ (a, b, c) and the mesh grid (d) of Example 2 for $N = 1243$ and $\eta \approx 7 \times 10^{-3}$

it in Fig. 4. No H^1 or L^2 errors are shown because we have no analytical solution here. As expected, the a posteriori error estimator converges to the optimal order from the related theory, i.e., $\mathcal{O}(N^{-1/2})$.

Example 3 In this example, we consider the effect of boundary layer or the thin Debye layer thickness, i.e., the general steady-state PNP (2) as follows: to find $p(\boldsymbol{x}), n(\boldsymbol{x}), \psi(\boldsymbol{x}) \in H_0^1(\Omega)$, such that

$$\begin{cases} -\Delta p - \nabla \cdot (p \nabla \psi) = f_1, \\ -\Delta n + \nabla \cdot (n \nabla \psi) = f_2, \\ -\epsilon \Delta \psi - p + n = f_3, \end{cases} \tag{75}$$

with $0 < \epsilon < 1$, and $\Omega = (0, 1) \times (0, 1)$. We take

$$\begin{cases} p = n = e^{-x/\sqrt{\epsilon}} + e^{-y/\sqrt{\epsilon}}, \\ \psi = e^{-3x/\sqrt{\epsilon}} + e^{-3y/\sqrt{\epsilon}}, \end{cases} \tag{76}$$

as an exact solution of (75) and typically choose $\epsilon = 10^{-1}$, 10^{-3} and 10^{-5}. The functions f_1, f_2 and f_3 on the RHS are determined by the exact solution.

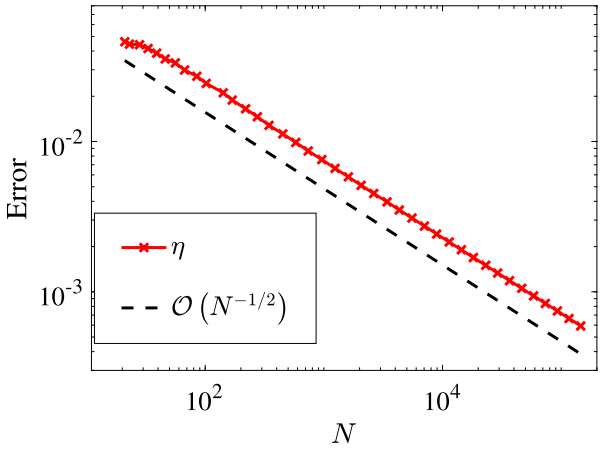

Fig. 4 The a posteriori error estimator η for Example 2 which converges to $\mathcal{O}\left(N^{-1/2}\right)$

For small values of ϵ, the exact solutions (76) shall predict obvious boundary layer effects near $x = 0$ and $y = 0$. We run the adaptive algorithm for $\epsilon = 10^{-1}$, 10^{-3} and 10^{-5} and show the results in Fig. 5. In panels (a, b, c), the consistent convergence of

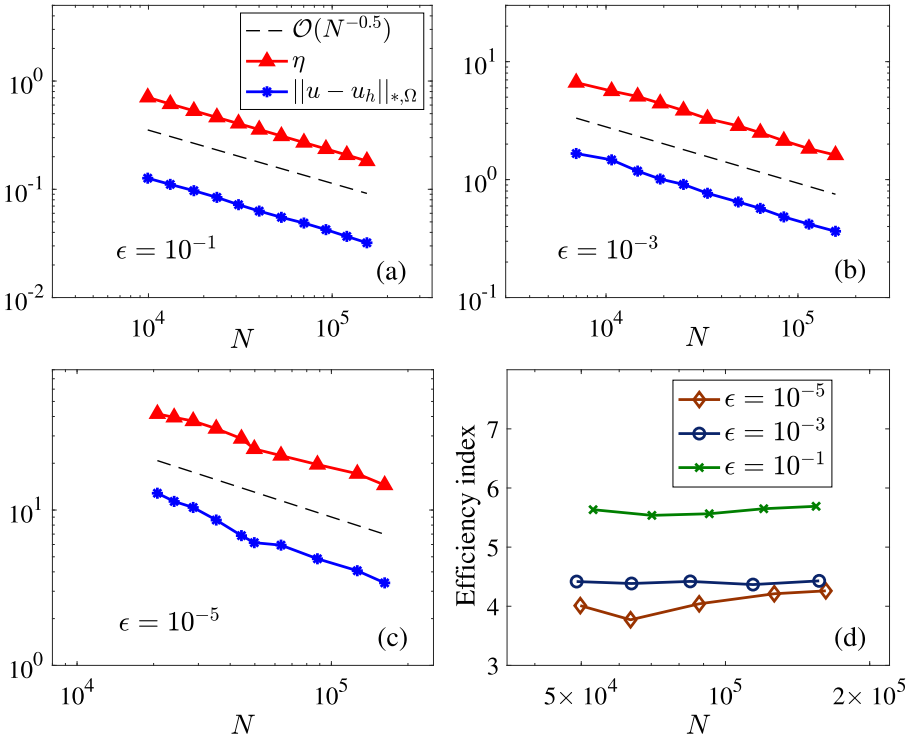

Fig. 5 (a, b, c) The a posteriori error estimator η and errors for Example 3 which converge to $\mathcal{O}\left(N^{-1/2}\right)$. (d) The corresponding efficiency indexes

the ϵ-dependent error and η for each case is observed as increasing N, i.e., $\mathcal{O}(N^{-1/2})$. As well known, an error estimator is considered to be efficient if the efficiency index $\eta/\|u - u_h\|_{*,\Omega}$ and its inverse remain bounded for all mesh sizes. Panel (d) here indicates that the error estimator is always efficient as the parameter ϵ gets smaller and smaller. Additionally, $\eta/\|u - u_h\|_{*,\Omega} = O(1)$ for all three cases, which shall demonstrate the robustness of our error estimator.

In order to illustrate the adaptivity of the mesh refinements, the corresponding mesh grids for typical degrees of freedom are presented in Fig. 6. Through panels (a, b, c) where degrees of freedom are close to each other, the adaptivity can be demonstrated as more condensed grids near the boundaries are visualized as ϵ is decreasing. In panel (c), we observed the much more condensed grids near the origin point (bottom left) than other parts of the boundaries, i.e., $x = 0$ and $y = 0$. This is attributed to the limited number of total grids ($N = 632$) and the priority of refinement near $(x, y) = (0, 0)$. As N is increased to be large enough, the mesh refinements are well observed near both $x = 0$ and $y = 0$, as shown in panel (d).

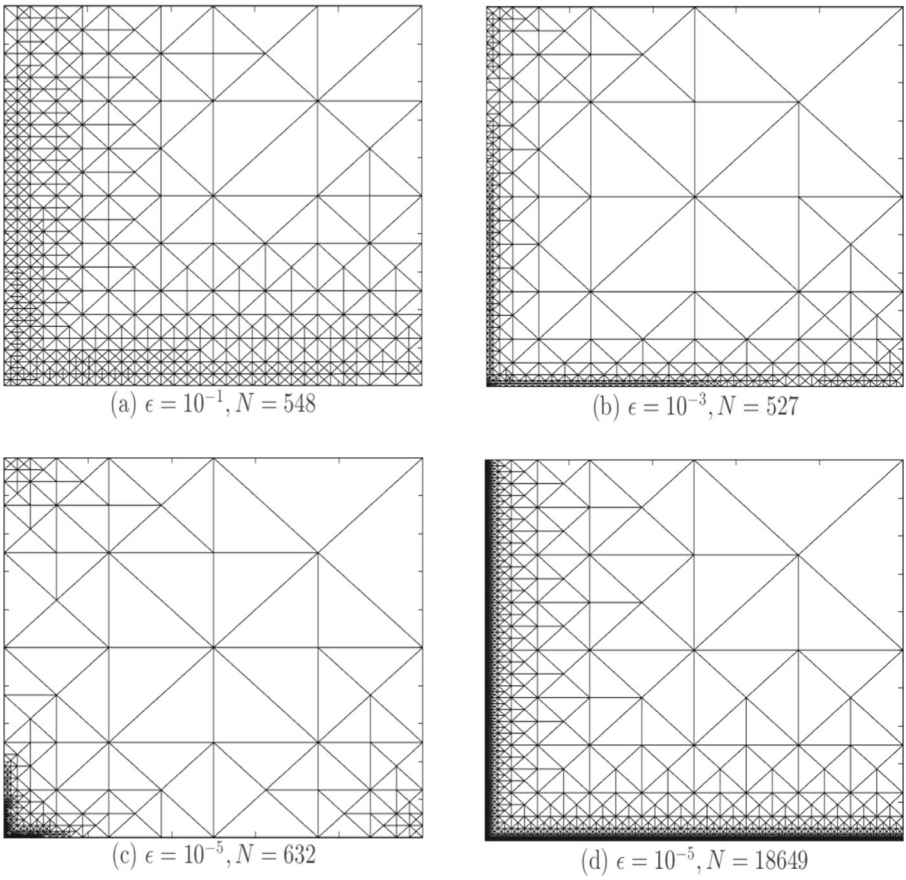

Fig. 6 The adaptive mesh grids for cases with different ϵ in Example 3

5 Conclusions

In this paper, the residual-based a posteriori error estimator has been adopted for the adaptive analysis of steady-state PNP equations where the nonlinearity and strong coupling are focused. During the theoretical study of the a posteriori error estimation, we have established the robust relationship between the a posteriori error estimator and the error of solution with the help of the regularity of the linearized system that is derived by taking G-derivatives of the nonlinear system, so as to demonstrate the efficiency and reliability of the error estimator.

We have successfully shown the rationality of theoretical conclusions by numerical results. The efficiency and reliability of the a posteriori error estimator are confirmed numerically in Examples 1 and 3. The adaptive performances with treating geometrical singularities and boundary layer effects are given in Examples 2 and 3, respectively. Nevertheless, in view of more thorough investigations that have not been done here, we only consider this work as a very starting point of adaptive methods for the PNP system. On the numerical side, to the authors' best knowledge, the convergence and stability of the entire adaptive algorithm for steady-state PNP has not been studied systematically, despite some of the existed methods [39, 67]. Last but not least, the general estimation analysis and the adaptive method for time-dependent PNP are of many more interests. Notably, the general adaptive method that includes the temporal adaptivity is more challenging and is our ongoing work.

Funding T. Hao and X. Xu received financial support from NSFC (No. 11671302). M. Ma received financial support from NSFC (No. 11701428), "Chen Guang" project supported by Shanghai Municipal Education Commission and Shanghai Education Development Foundation, and the Fundamental Research Funds for the Central Universities.

Data availability The datasets generated during and/or analysed during the current study are available from the corresponding author on reasonable request.

Declarations

Conflict of interest The authors declare no competing interests.

References

1. Adams, R.A.: Sobolev Spaces. Academic Press, New York (1975)
2. Ainsworth, M., Babuška, I.: Reliable and robust a posteriori error estimation for singularly perturbed reaction-diffusion problems. SIAM J. Numer. Anal. **36**(2), 331–353 (1999)
3. Ainsworth, M., Oden, J.T.: A posteriori error estimation in finite element analysis. Wiley, New York (2000)
4. Ainsworth, M., Vejchodský, T.: Fully computable robust a posteriori error bounds for singularly perturbed reaction-diffusion problems. Numer. Math. **119**(2), 219–243 (2011)
5. Barcilon, V., Chen, D., Eisenberg, R.S., Jerome, J.W.: Qualitative properties of steady-state Poisson-Nernst-Planck systems: perturbation and simulation study. SIAM J. Appl. Math. **57**(3), 631–648 (1997)
6. Binev, P., Dahmen, W., Devore, R.: Adaptive finite element methods with convergence rates. Numer. Math. **97**(2), 219–268 (2004)

7. Bolintineanu, D.S., Sayyed-Ahmad, A., Davis, H.T., Kaznessis, Y.N.: Poisson-Nernst-Planck models of nonequilibrium ion electrodiffusion through a protegrin transmembrane pore. PLOS Comput. Biol. **5**(1), e1000277 (2009)
8. Bousquet, A., Hu, X., Metti, M.S., Xu, J.: Newton solvers for drift-diffusion and electrokinetic equations. SIAM J. Sci. Comput. **40**(3), B982–B1006 (2018)
9. Brenner, S.C., Scott, L.R.: The mathematical theory of finite element methods. Springer (1998)
10. Brezzi, F., Capelo, A.C.S., Gastaldi, L.: A singular perturbation analysis of reverse-biased semiconductor diodes. SIAM J. Math. Anal. **20**(2), 372–387 (1989)
11. Brezzi, F., Marini, L.D., Micheletti, S., Pietra, P., Sacco, R., Wang, S.: Discretization, of semiconductor device problems. Handb. Numer. Anal. **13**, 317–441 (2005)
12. Bubuka, I., Vogelius, M.: Feedback and adaptive finite element solution of one-dimensional boundary value problems. Numer. Math. **44**(1), 75–102 (1984)
13. Cárdenas, A.E., Coalson, R.D., Kurnikova, M.G.: Three-dimensional Poisson-Nernst-Planck theory studies: influence of membrane electrostatics on gramicidin a channel conductance. Biophys. J. **79**(1), 80–93 (2000)
14. Carstensen, C., Dolzmann, G.: A posteriori error estimates for mixed finite element method in elasticity. Numer. Math. **81**(2), 187–209 (1998)
15. Cheddadi, I., Fučik, R., Prieto, M.I., Vohralik, M.: Guaranteed and robust a posteriori error estimates for singularly perturbed reaction-diffusion problems. ESAIM-Math. Model. Num. **43**(5), 867–888 (2009)
16. Chen, L., Holst, M., Xu, J.: The finite element approximation of the nonlinear Poisson-Boltzmann equation. SIAM J. Numer. Anal. **45**(6), 2298–2320 (2007)
17. Ciarlet, P.: The finite element method for elliptic problems. Publishing Company, North-Holland (1978)
18. Demlow, A., Kopteva, N.: Maximum-norm a posteriori error estimates for singularly perturbed elliptic reaction-diffusion problems. Numer. Math. **133**(4), 707–742 (2016)
19. Ding, J., Wang, Z., Zhou, S.: Positivity preserving finite difference methods for Poisson-Nernst-Planck equations with steric interactions: Application to slit-shaped nanopore conductance. J. Comput. Phys., 108864 (2019)
20. Dione, I., Doyon, N., Deteix, J.: Sensitivity analysis of the Poisson-Nernst-Planck equations: a finite element approximation for the sensitive analysis of an electrodiffusion model. J. Math. Biol., 1–36 (2018)
21. Dörfler, W.: A convergent adaptive algorithm for Poisson's equation. SIAM J. Numer. Anal. **33**(3), 1106–1124 (1996)
22. Eriksson, K., Johnson, C.: Error estimates and automatic time step control for nonlinear parabolic problems, I. SIAM J. Numer. Anal. **24**(1), 12–23 (1987)
23. Gajewski, H.: On uniqueness and stability of Steady-State carrier distributions in semiconductors. Springer, Berlin (1986)
24. Gajewski, H., Groger, K.: On the basic equations for carrier transport in semiconductors. J. Math. Anal. Appl. **113**(1), 12–35 (1986)
25. Gao, H., Sun, P.: A linearized local conservative mixed finite element method for Poisson-Nernst-Planck equations. J. Sci. Comput. **77**(2), 793–817 (2018)
26. Golovnev, A., Trimper, S.: Steady state solution of the Poisson-Nernst-Planck equations. Phys. Lett. A **374**(28), 2886–2889 (2010)
27. Golovnev, A., Trimper, S.: Analytical solution of the Poisson-Nernst-Planck equations in the linear regime at an applied dc-voltage. J. Chem. Phys. **134**(15), 154902 (2011)
28. Hayeck, N., Nachaoui, A., Nassif, N.R.: Existence and regularity for Van Roosbroeck systems with general mixed boundary conditions. Compel. **9**(4), 217–228 (1990)
29. He, M., Sun, P.: Mixed finite element analysis for the Poisson-Nernst-Planck/Stokes coupling. J. Comput. Appl. Math. **341**, 61–79 (2018)
30. Hollerbach, U., Chen, D.P., Eisenberg, R.S.: Two- and three-dimensional Poisson-Nernst-Planck simulations of current flow through gramicidin A. J. Sci. Comput. **16**(4), 373–409 (2001)
31. Holst, M., Baker, N.A., Wang, F.: Adaptive multilevel finite element solution of the Poisson-Boltzmann equation I: Algorithms and examples. J. Comput. Chem. **21**(15), 1319–1342 (2000)
32. Horng, T., Lin, T., Liu, C., Eisenberg, B.: PNP equations with steric effects: A model of ion flow through channels. J. Phys. Chem. B **116**(37), 11422–11441 (2012)

33. Hu, J., Huang, X.: A fully discrete positivity-preserving and energy-dissipative finite difference scheme for Poisson–Nernst–Planck equations. Numer. Math., 1–39 (2020)
34. Jasielec, J.J., Filipek, R., Szyszkiewicz, K., Fausek, J., Danielewski, M., Lewenstam, A.: Computer simulations of electrodiffusion problems based on Nernst-Planck and Poisson equations. Comp. Mater. Sci. **63**(none), 75–90 (2012)
35. Jerome, J.W.: Consistency of semiconductor modeling: An existence/stability analysis for the stationary Van Roosbroeck system. SIAM J. Appl. Math. **45**(4), 565–590 (1985)
36. Jerome, J.W., Kerkhoven, T.: A finite element approximation theory for the drift diffusion semiconductor model. SIAM J. Numer. Anal. **28**(2), 403–422 (1991)
37. Jiang, J., Cao, D., Jiang, D.E., Wu, J.: Time-dependent density functional theory for ion diffusion in electrochemical systems. J. Phys. Condens. Mat. **26**(28), 284102 (2014)
38. Kilic, M.S., Bazant, M.Z., Ajdari, A.: Steric effects in the dynamics of electrolytes at large applied voltages. II. modified Poisson-Nernst-Planck equations. Phys. Rev. E **75**(2), 021503 (2007)
39. Li, Y.: Analysis of novel adaptive two-grid finite element algorithms for linear and nonlinear problems. arXiv:1805.07887 (2018)
40. Lions, J.L., Magenes, E.: Nonhomogeneous boundary value problems and applications. Springer, New York (1970)
41. Liu, H., Wang, Z.: A free energy satisfying discontinuous galerkin method for one-dimensional Poisson-Nernst-Planck systems. J. Comput. Phys. **328**, 413–437 (2017)
42. Liu, W.: Geometric singular perturbation approach to steady-state Poisson-Nernst-Planck systems. SIAM J. Appl. Math. **65**(3), 754–766 (2005)
43. Lu, B., Holst, M., Mccammon, J.A., Zhou, Y.: Poisson-Nernst-Planck, equations for simulating biomolecular diffusion-reaction processes I: Finite element solutions. J. Comput. Phys. **229**(19), 6979–6994 (2010)
44. Lu, B., Zhou, Y.: Poisson-Nernst-Planck equations for simulating biomolecular diffusion-reaction processes II: Size effects on ionic distributions and diffusion-reaction rates. Biophys. J. **100**(10), 2475–2485 (2011)
45. Lu, B., Zhou, Y., Huber, G.A., Bond, S.D., Holst, M.J., Mccammon, J.A.: Electrodiffusion: a continuum modeling framework for biomolecular systems with realistic spatiotemporal resolution. J. Chem. Phys. **127**(13), 135102 (2007)
46. Mathur, S.R., Murthy, J.Y.: A multigrid method for the Poisson-Nernst-Planck equations. Int. J. Heat. Mass. Tran. **52**(17), 4031–4039 (2009)
47. Mauri, A., Bortolossi, A., Novielli, G., Sacco, R.: 3D, finite element modeling and simulation of industrial semiconductor devices including impact ionization. J. Math. Ind. **5**(1), 1 (2015)
48. Metti, M.S., Xu, J., Liu, C.: Energetically stable discretizations for charge transport and electrokinetic models. J. Comput. Phys. **306**, 1–18 (2016)
49. Mock, M.S.: Analysis of mathematical models of semiconductor devices. Boole Press, Dublin (1983)
50. Morin, P., Nochetto, R.H., Siebert, K.G.: Data oscillation and convergence of adaptive FEM. SIAM J. Numer. Anal. **38**(2), 466–488 (2001)
51. Schonke, J.: Unsteady analytical solutions to the Poisson-Nernst-Planck equations. J. Phys. A-Math. Theor. Math. Comp. **45**(45), 455204 (2012)
52. Singer, A., Gillespie, D., Norbury, J., Eisenberg, R.S.: Singular perturbation analysis of the steady-state Poisson-Nernst-Planck system: Applications to ion channels. Eur. J. Appl. Math. **19**(5), 541–560 (2008)
53. Song, Y., Zhang, Y., Bajaj, C.L., Baker, N.A.: Continuum diffusion reaction rate calculations of wild-type and mutant mouse acetylcholinesterase: Adaptive finite element analysis. Biophys. J. **87**(3), 1558–1566 (2004)
54. Song, Y., Zhang, Y., Shen, T., Bajaj, C.L., Mccammon, J.A., Baker, N.A.: Finite element solution of the steady-state Smoluchowski equation for rate constant calculations. Biophys. J. **86**(4), 2017–2029 (2004)
55. Tu, B., Xie, Y., Zhang, L., Lu, B.: Stabilized finite element methods to simulate the conductances of ion channels. Comput. Phys. Commun. **188**, 131–139 (2015)
56. Verfürth, R.: A posteriori error estimators for the Stokes equations. Numer. Math. **55**(3), 309–325 (1989)
57. Verfürth, R.: A posteriori error estimates for nonlinear problems. Finite element discretizations of elliptic equations. Math. Comp. **62**(206), 445–475 (1994)

58. Verfürth, R.: A posteriori error estimation and adaptive mesh-refinement techniques. J. Comput. Appl. Math. **50**(1C3), 67–83 (1996)
59. Verfürth, R.: Robust a posteriori error estimators for a singularly perturbed reaction-diffusion equation. Numer. Math. **78**(3), 479–493 (1998)
60. Wei, G.W., Zheng, Q., Chen, Z., Xia, K.: Variational multiscale models for charge transport. SIAM Rev. **54**(4), 699–754 (2012)
61. Wu, J., Srinivasan, V., Xu, J., Wang, C.: Newton-Krylov-Multigrid algorithms for battery simulation. J. Electrochem. Soc. **149**(10), A1342–A1348 (2002)
62. Xie, Y., Cheng, J., Lu, B., Zhang, L.: Parallel adaptive finite element algorithms for solving the coupled electro-diffusion equations. Mol. Based Math. Biol. **1**, 90–108 (2013)
63. Xu, J.: A new class of iterative methods for nonselfadjoint or indefinite problems. SIAM J. Numer. Anal. **29**(2), 303–319 (1992)
64. Xu, J., Zikatanov, L.: A monotone finite element scheme for convection-diffusion equations. Math. Comput. **68**(228), 1429–1446 (1999)
65. Xu, S., Chen, M., Majd, S., Yue, X., Liu, C.: Modeling and simulating asymmetrical conductance changes in gramicidin pores. Mol. Based Math. Biol. **2**(1), 34–55 (2014)
66. Xu, Z., Ma, M., Liu, P.: Self-energy-modified Poisson-Nernst-Planck equations: WKB approximation and finite-difference approaches. Phys. Rev. E **90**(1), 013307 (2014)
67. Yang, Y., Lu, B., Xie, Y.: A decoupling two-grid method for the steady-state Poisson-Nernst-Planck equations. arXiv:1609.02277 (2016)
68. Zeidler, E.: Nonlinear functional analysis and its applications. Springer, Berlin (1988)
69. Zhang, B., Chen, S., Zhao, J.: Guaranteed a posteriori error estimates for nonconforming finite element approximations to a singularly perturbed reaction-diffusion problem. Appl. Numer. Math. **94**, 1–15 (2015)
70. Zhao, J., Chen, S.: Robust a posteriori error estimates for conforming discretizations of a singularly perturbed reaction-diffusion problem on anisotropic meshes. Adv. Comput. Math. **40**(4), 797–818 (2014)
71. Zheng, Q., Chen, D., Wei, G.W.: Second-order Poisson-Nernst-Planck solver for ion channel transport. J. Comput. Phys. **230**(13), 5239–5262 (2011)
72. Zhou, Y., Lu, B., Huber, G.A., Holst, M.J., McCammon, J.A.: Continuum simulations of acetylcholine consumption by acetylcholinesterase: A Poisson-Nernst-Planck approach. J. Phys. Chem. B **112**(2), 270–275 (2008)